

**UNIVERSIDAD DE INVESTIGACIÓN DE
TECNOLOGÍA EXPERIMENTAL YACHAY**

Escuela de Ciencias Biológicas e Ingeniería

**TÍTULO: CHARACTERIZATION OF
POLYVINYLPIRROLIDONE NANOCOMPOSITES FIBERS
WITH MULTI-WALLED CARBON NANOTUBES.**

Trabajo de integración curricular presentado como requisito para la
obtención del título de Ingeniero Biomédica

Author:

Quizhpe Montesdeoca Ernesto Mateo

Advisor:

Dr. rer. nat. Julio C. Chacón Torres

Co-advisor:

Ph.D Sarah Elisa Briceño

Urcuquí, abril del 2024

AUTORÍA

Yo, **Quizhpe Montesdeoca Ernesto Mateo**, con cédula de identidad 0104721154, declaro que las ideas, juicios, valoraciones, interpretaciones, consultas bibliográficas, definiciones y conceptualizaciones expuestas en el presente trabajo; así como, los procedimientos y herramientas utilizadas en la investigación, son de absoluta responsabilidad de el/la autora (a) del trabajo de integración curricular. Así mismo, me acojo a los reglamentos internos de la Universidad de Investigación de Tecnología Experimental Yachay.

Urququí, abril del 2024.

Ernesto Mateo Quizhpe Montesdeoca

CI: 0104721154

AUTORIZACIÓN DE PUBLICACIÓN

Yo, **Quizhpe Montesdeoca Ernesto Mateo**, con cédula de identidad 0104721154, cedo a la Universidad de Investigación de Tecnología Experimental Yachay, los derechos de publicación de la presente obra, sin que deba haber un reconocimiento económico por este concepto. Declaro además que el texto del presente trabajo de titulación no podrá ser cedido a ninguna empresa editorial para su publicación u otros fines, sin contar previamente con la autorización escrita de la Universidad.

Asimismo, autorizo a la Universidad que realice la digitalización y publicación de este trabajo de integración curricular en el repositorio virtual, de conformidad a lo dispuesto en el Art. 144 de la Ley Orgánica de Educación Superior

Urcuquí, abril del 2024

Ernesto Mateo Quizhpe Montesdeoca

CI: 0104721154

Dedicatoria

Dedicado a las personas que siguen construyendo el futuro de la humanidad con sus manos y su mente, y es a futura generación que mejorara el universo.

-Ernesto Mateo Quizhpe Montesdeoca-

Agradecimiento

Agradezco a todo el apoyo que me brindaron mis padres y todo el cariño de mis hermanos. Gracias a mi familia que son los más importante que puedo tener en esta vida. Gracias a esos buenos profesores de Yachay que supieron inculcar la curiosidad en la ciencia de los estudiantes.

-Ernesto Mateo Quizhpe Montesdeoca-

Resumen

Introducción: La generación de nuevos materiales para la sociedad ha ayudado a mejorar capacidades tecnológicas, ambientales, sociales, medicas, entre otras. Una parte fundamental y hablada los últimos años han sido las aplicaciones que se encuentran en los nanotubos de carbono (NC). Este material tiene campos prometedores por sus propiedades físicas como dureza, flexibilidad, duración y estabilidad. Al añadir polivinilpirrolidona (PVP), los NC forman un compuesto más biocompatible y con mejor flexibilidad y estabilidad. Pero su fabricación es deficiente, por lo que se usan diferentes métodos y compuestos catalizadores como nanopartículas de cobre (Cu NPs).

Metodología: En este estudio de caracterización se usos un compuesto conformado por multicapas de nanotubos de carbono (MWCNTs), PVP y Cu NPs. Se utilizo la técnica de espectroscopia raman, donde se usó cada muestra para analizar sus características. Para ello se usó distintos tamaños de las Cu NPs, de 5 a 25 nm. Subsecuentemente analizando su utilidad en la medicina y biomedicina.

Resultados y discusión: Se obtuvieron los diferentes valores de intensidad con las Cu NPs, donde destacaron los tamaños de 5 y 10 nm. Estos valores tenían intensidades mucho más altas en las bandas G, D, G* y enlaces de hidrogeno.

Conclusión: Se encontró que el compuesto de PVP/MWCNTs-CuNPs mejoro las características de cristalinidad, fuerza de enlaces, flexibilidad, resistencia y orden. Las aplicaciones para estos compuestos con características mejoradas fueron en campos como sensores de dopamina, anticoagulante y crecimiento neuronal.

Palabras Clave: Multicapas de nanotubos de carbono, polivinilpirrolidona, nanopartículas de cobre, biomedicina, espectroscopia raman.

Abstract

Introduction: The generation of new materials for society has helped improve technological, environmental, social, medical, and other capabilities. In recent years, a fundamental and widely discussed aspect has been the applications found in carbon nanotubes (CNTs). This material holds promising potential due to its physical properties such as hardness, flexibility, durability, and stability. By adding polyvinylpyrrolidone (PVP), CNTs form a more biocompatible compound with improved flexibility and stability. However, their manufacturing is deficient, leading to the utilization of various methods and catalytic compounds such as copper nanoparticles (Cu NPs).

Methodology: In this characterization study, a compound composed of multi-layered carbon nanotubes (MWCNTs), PVP, and Cu NPs was used. Raman spectroscopy technique was employed, where each sample was analyzed for its characteristics. Different sizes of Cu NPs, ranging from 5 to 25 nm, were utilized. Subsequently, their utility in medicine and biomedicine was analyzed.

Results and Discussion: Different intensity values were obtained with Cu NPs, with sizes of 5 and 10 nm standing out. These values exhibited significantly higher intensities in the G, D, G*, and hydrogen bond bands.

Conclusion: It was found that the PVP/MWCNTs-CuNPs compound improved characteristics such as crystallinity, bond strength, flexibility, resistance, and order. Applications for these compounds with enhanced features were found in fields such as dopamine sensors, anticoagulants, and neuronal growth.

Keywords: Multi-layered carbon nanotubes, polyvinylpyrrolidone, copper nanoparticles, biomedicine, Raman spectroscopy.

Contents

List of figures.....	i
List of tables.....	v
Chapter 1	1
1. Introduction	1
1.1. PVP.....	2
1.1.1 Molecular structure of PVP.....	3
1.1.2. PVP Synthesis	5
1.1.3 PVP properties	9
1.1.4. PVP SEM and Raman spectroscopy.....	11
1.1.4. PVP applications	12
1.2. Carbon-based materials	17
1.2.1. Atomic structure and morphology of carbon nanotubes	18
1.2.2. Multi-walled carbon nanotube.....	19
1.2.3. MWCNTs synthesis	21
1.2.4. MWCNTs properties	23
1.2.5. MWCNTs SEM and Raman spectroscopy	24
1.2.5. MWCNTs applications.....	26
1.3. MWCNTs/PVP	27
1.3.1. MWCNTs/PVP Synthesis	29
1.3.2. MWCNTs/PVP properties.....	30
1.3.3. MWCNTs/PVP applications	31
1.4. NP and solvent	34
1.4.1. CoFe ₂ O ₄ NP.....	34
1.4.2. N,N-dimetilformamida and ethanol.....	37
Chapter 2	39
2. Motivation	39
2.1. Problem statement.....	40
2.2. General and specific objectives	40
Chapter 3	41
3. Methodology.....	41

3.1. Optical microscopy	41
3.1.1. Fundamental principle of SEM	42
3.1.2. SEM process	42
3.2. Raman Spectroscopy	43
3.2.2. Raman spectroscopy process	44
3.2. Synthesis of MWCNT/PVP with COF in Germany	45
3.1.1 COF NP synthesis	45
3.1.1. PVP/MWCNTs synthesis	46
3.1.2. PVP/MWCNTS characterization in Germany	47
Chapter 4	41
4. Results & Discussion.....	48
4.1 Raman spectra and microscope images	48
4.1.1. PVP Raman spectra and microscope images	49
4.1.2. MWCNTs/PVP Raman spectra and microscope images	50
4.1.2. MWCNTs/PVP/CoFe ₂ O ₄ Raman spectra and microscope images	51
Chapter 5	54
5. Conclusions.....	54

List of figures

Figure 1. a) PVP powder, b) SEM image of PVP fibers

Figure 2. a) Structure of the repeating unit and b) three-dimensional structure of the PVP

Figure 3. In the X,Y and Z planes, the dielectric polar moments of the PVP structure are observed.

Figure 4. Prof. Dr. Walte Rappe showing the functionalization and polymerization process of NVP.

Figure 5. NVP generation and functionalization process. (Adapted from Rutgers, The State University of New Jersey)

Figure 6. a) Free radical-containing mechanisms and b) Hydroxy-containing mechanisms.

Figure 7. a) Rama spectroscopy and b) PVP SEM image with purity of 100%, 90% and 80%.

Figure 8. a) PVP coating process with Fe₃O₂, b) Addition of epoxy to the PVP/Fe₃O₂ functionalized particle, and c) TEM image of PVP/ Fe₃O₂/epoxy.biomedical particles.

Figure 9. Hydrogen bonding between acetaminophen/acetaminophen and PVP/acetaminophen

Figure 10. a) PVP- Carrageenan Blend Hydrogels, b) PVP- Carboxymethyl Cellulose (CMC) Blend Hydrogel and c)3D crosslinked porous structure in hydrogel.

Figure 11. a) PVP-CMC hydrogel applied in moist heat treatment and b) microporous PVP/PVA scaffold for the repair of focal articular cartilage defects

Figure 12. Molecular orbital theory applied in carbon atom.

Figure 13. Construction of the graphene layer, layer curl, with the chiral vector and the angle. Also, it shows your Armchair and Zig-Zag shape and vector latitudes a₁ and a₂.

Figure 14. a) Cylindrically curved coaxial, b) polygonal coaxial and c) scroll graphene sheet.

Figure 15. a) Arc-discharge Mechanism, b) MWCNTs 3D and Raman spectroscopy (L-band) and c) MWCNTs SEM image.

Figure 16. a) CVD mechanism, b) base growth model, c) tip-growth model and d) MWCNTs SEM image

Figure 17. a) shows the MAWCNTs Raman spectroscopy non-functionalize and functionalized and b) shows the MWCNTs Raman spectroscopy for aMWCNT and fMWCNT.

Figure 18. SEM image from MWCNTs fibers.

Figure 19. a) Process of cell proliferation in MWCNT/PEDOT matrix, growth after 2 days and differentiation after 5 days, b) matrix parts and scheme of muscle contraction, after 7 days the muscle can contract, c) muscle contraction in vitro and d) control of cell proliferation in MWCNT/PEDOT with electric stimulation.

Figure 20. a) SEM image of CS/MWCNT scaffolds from 200 μm to 5 μm and b) To obtain cell proliferation, Fluo-4 was applied, which stains the cells to be observed; control was performed in glass and the test in MWCNTs/CS. The fluctuation of fluorescence that is obtained is plotted against time; also, four specific cells were labeled to compare their proliferation activity

Figure 21. a) Show bond between hydroxyl group from MWCNT with oxygen from PVP and b) morphological binding of PVP on MWCNTs.

Figure 22. In the image is possible distinguish the hydrogen bond, that was functionalized, in contrast with solvent dispersion on CNTs

Figure 23. Process to attach the PVP on MWCNTs, it is use Tris-HCL with 8,5 pH, and the it heated by 48h at 30 $^{\circ}\text{C}$

Figure 24. a) the heating mechanism of the MWCNTs with the PVP layers acting as support, b) load distribution system to send current to the MWCNTs and c) nanofiber MWCNTs with different steps.

Figure 25. SEM image of MWCNTs with different concentration (0,6% and 0,1) with PVP

Figure 26. Analysis of proliferation in different matrix: control, SWCNT-COOH, MWCNT-COOH and MWCNT-PVP.

Figure 27. a) Grown of neuronal cells in MWCNTs/PVP, b) snail ringer in MWCNT where solution poise on glass and c) SEM to Analyse MWCNT topography.

Figure 28. a) process of thermal decomposition method and b) dispersion of nanoparticles and their average diameter.

Figure 29. When aggregate the NPs at the MWCNTs/PVP could be happen these two situations: dispersion or aggregation

Figure 30. a) SEM image and b) Raman spectrum of COF NP.

Figure 31. a) DMF and b) ethanol molecules

Figure 32. Raman spectrum and SEM imagen of PVP diluted in DMF and ethanol.

Figure 33. Secondary electron process for SEM.

Figure 34. SEM device, principle and detents process to obtain de image.

Figure 34. a) These vibration differences between each link will produce different changes in the photon frequency, which will help determine the properties of the material and b) three different reaction of fundamental Raman principle.

Figure 36. Raman spectroscopy device, each parts process where light is reflected to obtain the different masseurs

Figure 37. Similitudes between phenyl and benzyl.

Figure 38. Electrospinning machines with principal components: needle, (b) pump, (c) camera and (d) square collector covered with aluminum.

Figure 39. PVP with internal MWCNT, result from experiment analyzed in SEM

Fig 40. PVP Raman spectra a) shows the SEM image of the PVP, the green point is the area where the Raman spectroscopy data were obtained; b) Raman spectroscopy of the PVP

Figure 41. MWCNTs/PVP Raman spectra a) shows the SEM image of the MWCNTs/PVP, the green point is the area where the Raman spectroscopy data were obtained; b) Raman spectroscopy of the MWCNTs/PVP

Figure 42. MWCNTs/PVP SEM image with COF NPs a) fibers with NPs of 5 nm; b) fibers with NPs of 10 nm; c) fibers with NPs of 15 nm and d) fibers with NPs of 25 nm

Figure 43. Raman spectra of MWCNT/PVP with COF in each different size (5,10,15 and 25 nm)

List of tables

Table 1. Different PVP properties

Table 2. Different characteristics of some PVP with different K values from 15 to 90, for powder and aqueous solution stages

Table 3. Different applications of PVC for the industrial area and its scope in everyday products

Table 4. Difference between SWCNT and MWCNT.

Table 5. Some physics properties of MWCNTs

Table 6. Properties of ethanol and DMT

Chapter 1

1. Introduction

The development and study of materials have been very useful for the advancement of society, it could be thought that it starts from alchemy; but, even the Egyptians, with the manufacture of glass, already analyzed the elements of their environment. A clear example of these events is the discovery of rubber in 1839, which helped to generate a large amount of technology such as raincoats, insulation or tires. Furthermore, by analyzing and understanding the properties of each developed compound, it helps us to improve its mechanical, physical or chemical capabilities.(1,3)

These principles lead us to a particular nanostructure based on carbon, specifically carbon nanotubes (CNTs). Since its accidental discovery in 1991, several ways have been found to apply

its properties in different fields of science.(4) These nanotubes arise from the rolling of a layer of graphene; and, by winding one CNT inside another, several times, what are known as Multi Walled Carbon Nanotubes (MWCNTs) are generated. Despite not being the only way to configure carbon atoms, MWCNTs are molecules with properties of high hardness, flexibility, mechanical resistance and elasticity. For this reason, many scientists have studied and improved the capabilities of MWNTCs, finding applications in medicine as biochemical sensors or in physics as shielding materials for greater resistance.(1,5–7)

On the other hand, there is a particular compound, Poly-Vinyl-Pyrrolidone (PVP), developed in 1939.(8,9) PVP is a vinyl polymer that was originally used for the expansion of blood plasma in blood transfusion situations. Since its discovery, it has been associated in medical and industrial applications. The main characteristics of the compound are its low toxicity and biodegradability, in addition to serving as a disinfectant by combining PVP with Iodine. It is generally used in the implementation of adhesives, photo printing or excipients in pills.(3,10–12)

Therefore, with the great properties and low toxicity of this compound, it was decided to observe what characteristics can be obtained from them, and how they can help in various fields of science and industry.

1.1. PVP

Poly(vinylpyrrolidone) (PVP) is known by various names such as 1-ethenylpyrrolidin-2-one, Povidone, Poly[1-(2-oxo-1-pyrrolidinyl) ethylene], among others. PVP was first patented in Germany in 1939 by scientist Walter J. Reppe.(13) This compound is a polymer lineal that is obtained by joining various vinylpyrrolidone (VP) monomers; thus, obtaining a compound resistant to temperature, non-toxic, non-ionic, among other characteristics(3). Containing malleable and easy handle properties, it has found applications in various fields such as pharmacology, medicine, biomedicine, the textile industry or even photography. On macro scale it has a form of powder, and under the microscope a granular form; although, in general, it is obtained as fibers. (Fig. 1)(14)

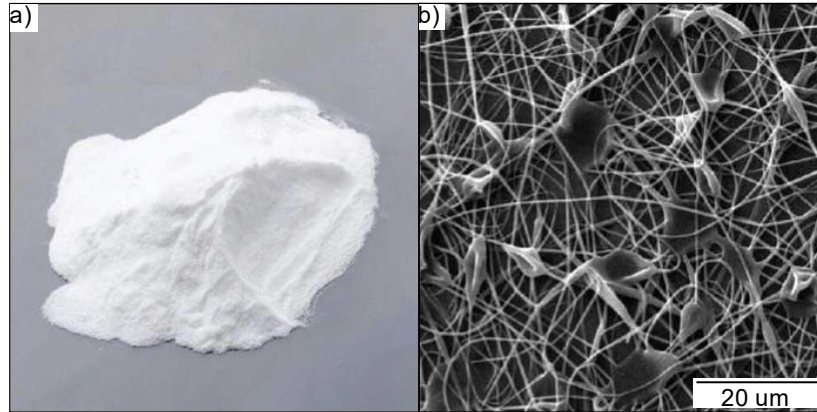


Figure 1. a) PVP powder, b) SEM image of PVP fibers (adapted from *International Journal of Thermophysics and Biosensors Journal*)(14,15)

1.1.1 Molecular structure of PVP

For molecular structure, PVP is built from vinylpyrrolidone chains, and it join with single covalent bonds between each carbon. The monomer is made up of 1 oxygen, 1 nitrogen, 6 carbons, and 9 hydrogens, and the chain creates linkages at the extreme methane molecules.(3) Therefore, its molecular formula is $(C_6H_9NO)_n$ with single bonds except for O, which forms an ionic double bond with the fourth carbons. (8,9) Since PVP can have certain variations in its size relative to its viscosity, it has a mass molar between 2,500 to 2,500,000 g.mol⁻¹. In addition, it has a balance of hydrophilic and hydrophobic groups in its structure that provides its solvent properties. (Fig. 2)(16,17)

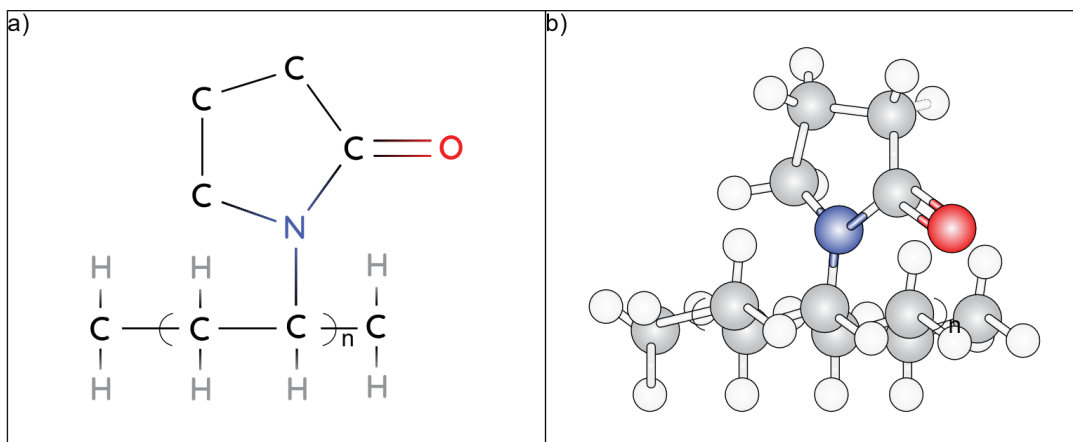


Figure 2. a) Structure of the repeating unit and b) three-dimensional structure of the PVP

On the other hand, the study of the behavior of PVP in polar solvents reflects a complex challenge, since experiments carried out at the Materials Physics Unit, Joint Center and Materials Physics Department of the University of the Basque Country demonstrated the difficulty of observing of polymer chains in dielectric states.(18) In this way, the analysis of these polymers is compromised, since their chain frequencies are much lower, detecting these errors. Therefore, there is a need to analyze the polar moments of the bonds in order to determine a suitable PVP structure, and the bond dipole is given by the formula [1] (19,20):

$$[1] \quad \mu = \delta \cdot d$$

For this, the $+\delta/\delta-$ bonds are modeled, and d representing the distance that will be measured in Angstroms (\AA). Finally, the values obtained from the study of the electric dipole moment will be determined in Debye (D), which is approximately $3.33564 \times 10^{-30} \text{ C}\cdot\text{m}$. (19)

Figure 3 shows in more detail the composition of dipole moments in relation to their position. This graph captures the state of minimum energy in its conformation, where the chain runs along the Z axis, the bond of C with the polymeric chain and the nitrogen are plotted on the Y axis and finally the C, N and O in the side group are lie in the XY plane. When analyzing its structure, a permanent dipole moment with a magnitude of 3.53 D is found.

The bond between the C of the polymeric chain and the N perpendicular to the chain shows an angle of 78° between its dipole moments. In addition, the type B dipole moment of 0.73 D lying perpendicular to the main chain contour as a magnitude of the fixed dipole moment. This section is important as it shows the glass transition phenomenon that fluctuates to micro-Brownian motion for the PVP.(3,9) In contrast, looking from the pendant side group to the polymeric chain, being type C, a magnitude of 3.45 D is known, which is perpendicular to type B. In this way, a direct connection is generated, formed by a covalent bond of N with C. With these results studied, it was possible to determine the dynamics of PVP in polar solvents at Tokai University.(18,21)

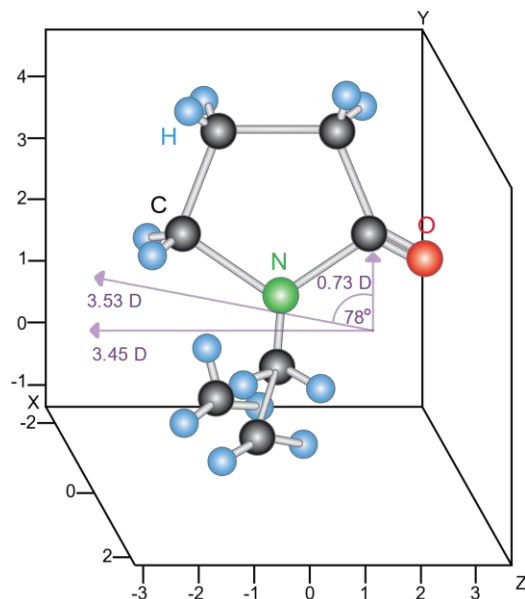


Figure 3. In the X,Y and Z planes, the dielectric polar moments of the PVP structure are observed.(adapted from Macromolecules Journal)(21)

1.1.2. PVP Synthesis

The German conglomerate IG Farber, with the help of Prof. Dr. Walte Rappe and his team, pioneered the development of PVP. Research in the field of acetylene generated various processes and synthesis of chemicals and materials. (9,22)At that time, acetylene could only be used below 1.5 bar, since it decomposes explosively at higher temperatures, which is why Rappe sought to handle acetylene at pressures up to 25 bar; thus, this synthesis is known as Rappe chemistry. (Fig 3)(22,23)

Firstly, Rappe's functional team raised the VP in N-vinipyrrolidone (NVP), and then successfully polymerized it to obtain the semicrystalline PVP, which had a flexible and coiled chain.(18,24) In this way, a polymer was obtained that was soluble in water or saline water with a concentration of 3.5%, being isotonic for blood plasma.(23,24)

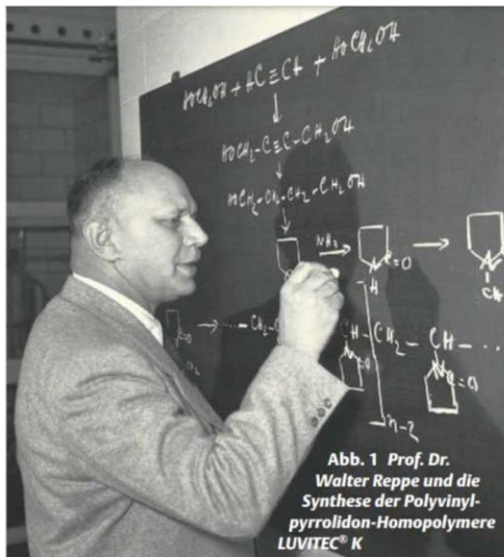
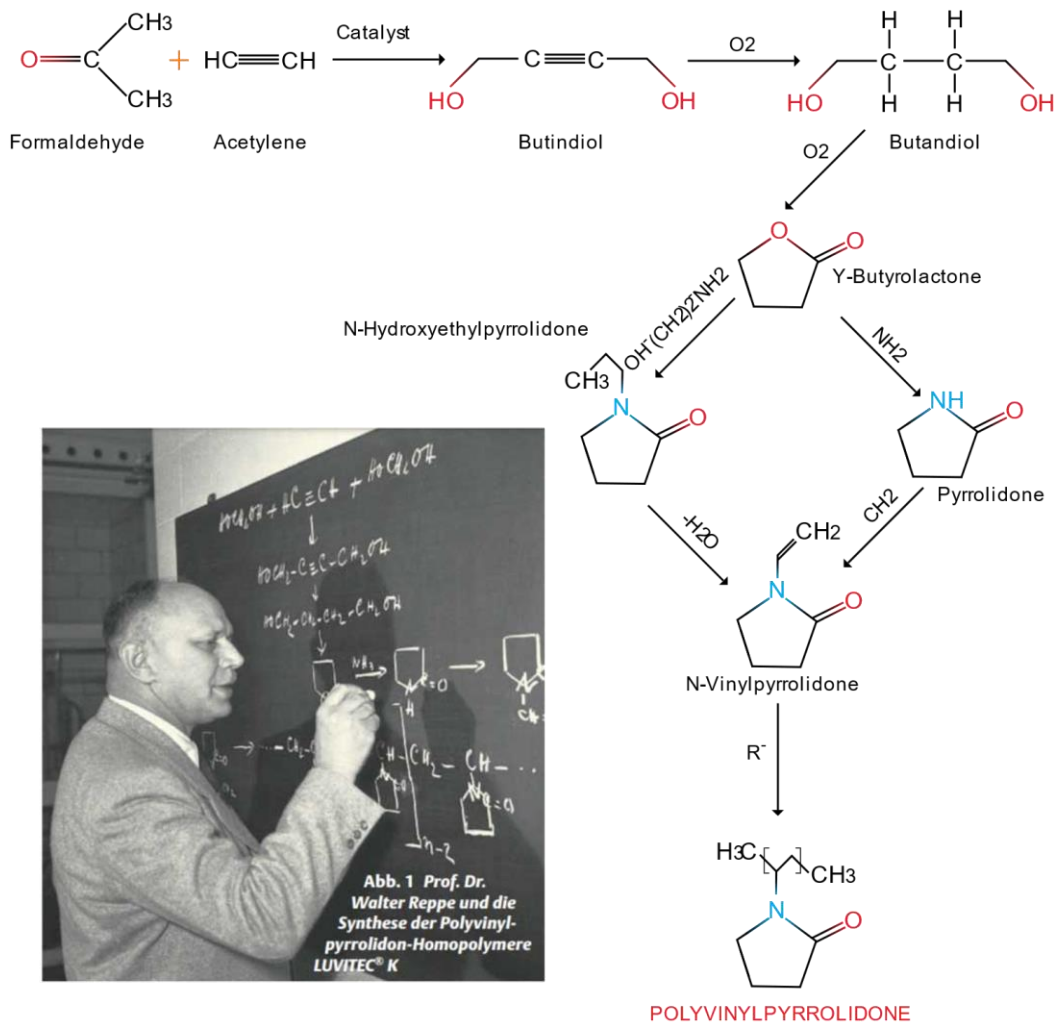


Figure 4. Prof. Dr. Walte Rappe showing the functionalization and polymerization process of NVP. (adapted from Inter Science) (23)

1.1.2.1. Synthesis process by acetylation.

For the synthesis of NVP, it must go through four working processes: ethynylation, cyclization, hydro carboxylation and vinylation.(22) The synthesis starts with acetylene by the **ethynylation** process, formaldehyde is added at 300 to 350 psi with Cu-acetylide catalyst as catalyst to generate

butynediol. Then, this compound is hydrogenated, and when the compound is reduced, the intermediate double chain between carbons 1 and 3 is eliminated, with which 1,4-butanediol is obtained. To close the lactam ring, Cu-catalyst is added to the **cyclization** process, which will help to functionalize the 1,4-butanediol in γ -butyrolactone (GBL). (20,22,25)

From this point it is necessary to add output to the molecules to facilitate the bonding of the oxidative ring to nitrogen. Therefore, ammonia is added and the temperature is raised to 230°C obtaining 2-pyrrolidone, accelerating the **hydroxy carboxylation**. Finally, for NVP it is synthesized with acetylene in 2-Py, generating the **vinylation** or Reppe vinylation process, thus linking ethene to nitrogen. Thus, a simple functionalized VP monomer, which will bond with the next carbon of the monomer. (Fig. 5)(22–24,26,27)

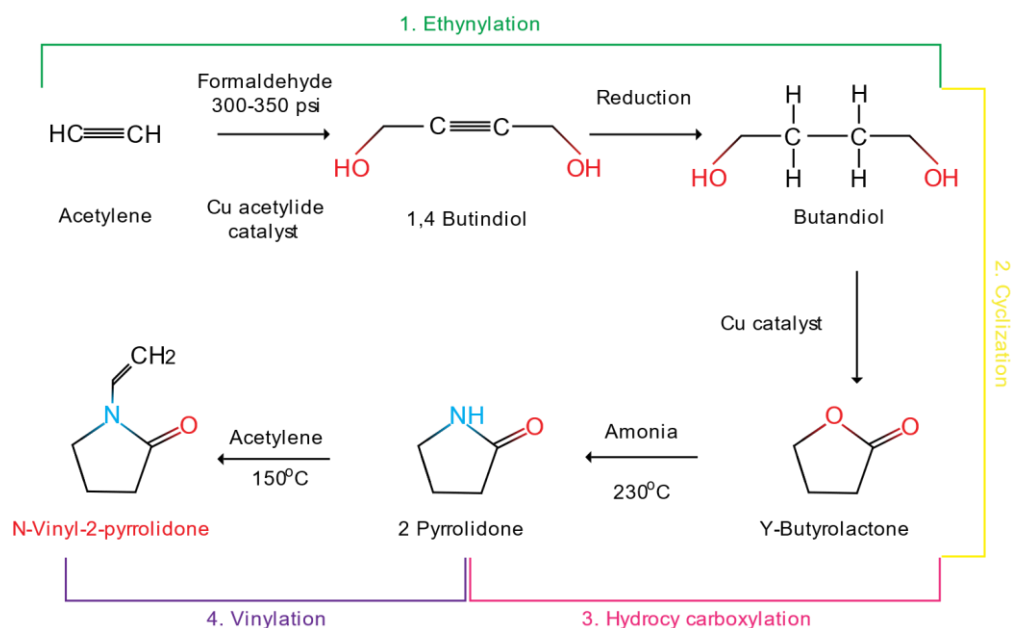


Figure 5. NVP generation and functionalization process. (Adapted from Rutgers, The State University of New Jersey)(24)

To generate the polymer chain, the chain-growth polymerization method is used, where the polymers are added one next to the other. There are some useful mechanisms for proper polymerization, for PVP two mechanisms can be used: free radical-containing mechanisms and hydroxy-containing mechanisms.(28)

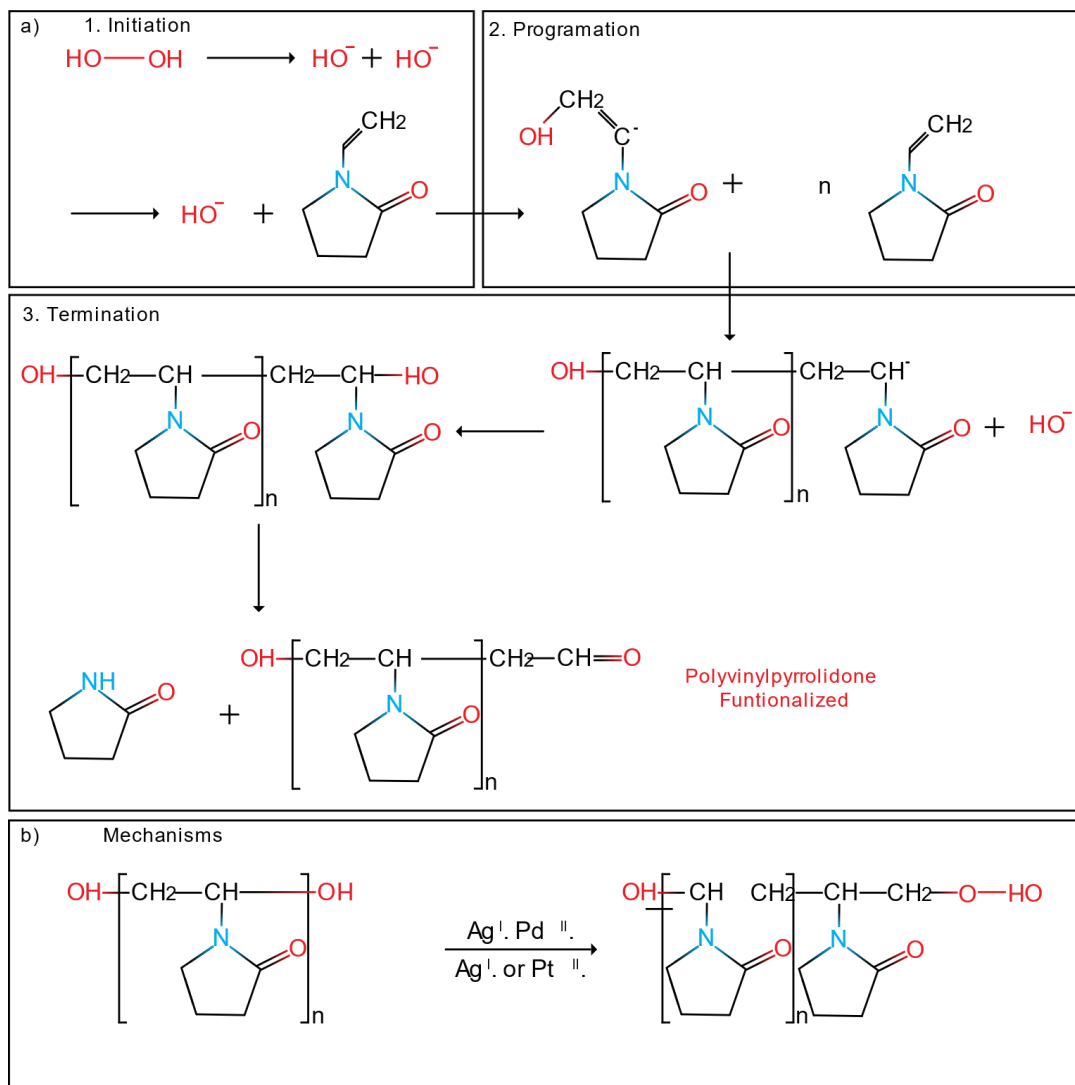


Figure 6. a) Free radical-containing mechanisms and b) Hydroxy-containing mechanisms (adapted from Polymer review)(28,31)

- 1) Free radical-containing mechanisms is basically a reduction between polymers and metal ions, for example gold, which will have free radicals as intermediates. For the covalent bond between carbon and hydrogen, free radicals are used that will break this bond. In this way, nanoparticles (NP) are generated from these metals and a free proton. Figure 6a shows this process demonstrated by Hoppe at the Laboratory of Magnetism and Nanotechnology

at the University of Santiago de Compostela. For reaction 1 there is direct abstraction of hydrogen with the help of the metal ion taken from the polymer. On the other hand, point 2 shows the reduction of the metal precursor with the help of radicals during the degradation of PVP.(29,30)

- 1) Hydroxy-containing mechanisms consist of the use of noble metals such as Ag (I), Au (III), Pd (II) or Pt (II) that will generate an exchange of electrons as shown in figure 6b. With these metals the PVP will have three alternatives in which an electron would be transferred by means of a radical, transfer of two electrons and two deprotonations of the alcohol or a deproteinization with a transfer to the metal ion by the hydride. Finally, this polymerization usually ends the chain with a hydroxyl group (OH).(30,31)

1.1.3 PVP properties

PVP properties	
Melting point	>300 °C
Boiling point	90-93 °C
Density	1,69 g/cm ³
storage temperature	2-8°C
solubility	H2O: soluble 100mg/mL
Form	Powder
Color	White to yellow-white
PH	3.0-5.0
Water Solubility	Soluble in water.
Sensitive	Hygroscopic
Merck	147697
Stability	Stable. Incompatible with strong oxidizing agents. Light sensitive. Hygroscopic.
Average molecular weight	8000-700000 Da

The

Table 1. Different PVP properties. (32-35)

Chemical Abstracts Service (CAS) and Substance Registry System (SRS), registers the compound with the number 9003-39-8 to determine its molecular properties.(17) There are mechanical,

physical, and chemical properties that help PVP find utility and acceptance in various parts of industry and medicine. One of its most important characteristics is its amphibian, that is, its ability to dissolve in polar and nonpolar solvents. On the part, the polar solvents are N,N-dimethylformamide (DMF), water and ethanol]; and on the part of the polar solvents are toluene, chloroform and dichloromethane, to mention a few.(31,32)

	Powder				Aqueous solution			
	PVP K-15	PVP K-30	PVP K-85	PVP K-90	PVP K-15 W	PVP K-30 W	PVP K-85 W	PVP K-90 W
Appearance	White powder	White powder	White powder	White powder	Clear viscous liquid	Clear viscous liquid	Clear viscous liquid	Clear viscous liquid
K-value * ¹	13.0~19.0	27.0~33.0	84.0~88.0	88.0~96.0	13.0~19.0	27.0~33.0	86.0~90.0	90.0~103.0
Solid content, %	≥95.0	≥95.0	≥95.0	≥95.0	19.0~21.0	29.0~31.0 49.0~51.0	19.0~21.0	19.0~21.0
Residual monomer content, ppm	<100	<100	<100	<100	<100	<100	<100	<100
pH	3.0~7.0	3.0~7.0	5.0~9.0	5.0~9.0	5.0~9.0	5.0~9.0	5.0~9.0	5.0~9.0
Water content (%)	<5.1	<5.0	<5.0	<5.0	-	-	-	-
Approximate molecular weight (Da)	8000	50000	200000	400000	8000	50000	200000	400000

Table 2. Different characteristics of some PVP with different K values from 15 to 90, for powder and aqueous solution stages (11,35)

Among the chemical properties is its stability against neutral and acid conditions.(34) However, the lactam ring in alkaline situations with high temperature decomposes. On the other hand, the

physical properties show strong dipole-dipole bonding. The hygroscopicity shows a balance in the absorption of 40%-80% atmospheric humidity. (Table 1)(32–34)

For commercial PVP, it usually has special characteristics that are determined by the degrees of polymerization that will give the molecular weights. For this part, the viscosity that the PVP can have due to the interaction of its polymeric chains is taken into account. (10,11) This value is represented by the letter K and its value varies from 10 to 120. For instance, PVP K-30 can be manufactured by spray drying as a sphere; but, if the value is higher, drum drying with plates is used. The PVP with granules that have greater fluidity are those of K25,30,90. (Table 2)(11,35)

To obtain K value, it is necessary to have the Fikentshcer value, which will give the viscosity related to the molecular weight (K). The following Fikentshcer formula is used to determine these values having the PVP at 25 °C [2]:

$$[2] \quad K = 1000 \cdot \frac{1,5 \log \eta_{rel} - 1 + \sqrt{1 + \left(\frac{2}{c} + 2 + 1,5 \log \eta_r\right) \cdot 1,5 \log \eta_{rel}}}{150 + 300c}$$

η_{rel} : Relative viscosity of the aqueous solution of PVP to water

c: Content (w/w%) of PVP in aqueous solution of PVP.(11)

Calculating the viscosity of the PVP will determine the proper formation of the fiber, given that, if it is highly viscous, it will generate very fragile defined fibers and if it is not very viscous it will not be able to generate a mesh and therefore the fibers due to their liquid state.

1.1.4. PVP SEM and Raman spectroscopy

The Raman spectrum of PVP shows peaks in the regions of 560, 754-1023, 1296, 1380-1494, 1662-300 and 330 cm⁻¹. Where the vibrations of the bonds for carbon, nitrogen, oxygen and hydrogen would be obtained. (11,36) Previous studies have shown that solvent and polymer concentrations determine whether the electrospinning solution can be electrochemically converted into nanofibers, which also has a significant effect on nanofiber morphology. Here, the hull spin electrolyte is prepared by dissolving PVP in aqueous ethanol.(20,35) This figure summarizes the SEM images of PVP nano electric filaments in different concentrations of ethanol and PVP, respectively. It is difficult to form discrete nanofibers with a low concentration of ethanol (80%), but a high concentration of ethanol will facilitate the production of PVP nanofibers, especially for pure ethanol. (Fig. 7)(22)

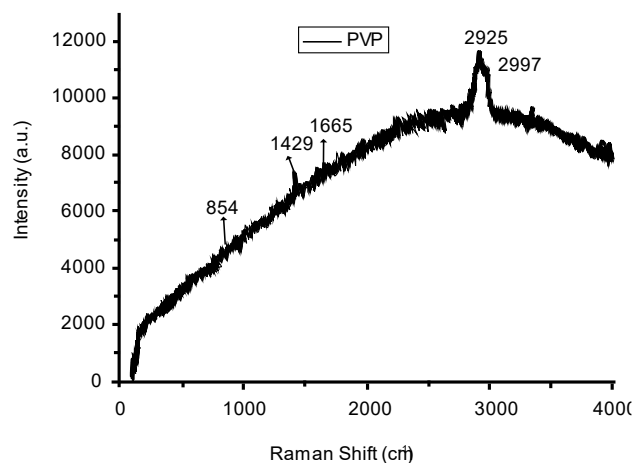


Figure 7. a) Raman spectroscopy and b) PVP SEM image with purity of 100%, 90% and 80%. (adapted from *Organic Chemistry*)(11)

1.1.4. PVP applications

1.1.4.1 Nanotechnology applications

PVP has the ability to mediate the transition from a metal to a NP, thanks to the previously mentioned process of Free Radical Containing Mechanisms. (Fig. 8a) The generation of magnetic Iron NPs, the best example for this synthesis. This site is generated apart from a co-precipitation (Fig. 8b), in this way the PVP is coated on the surface of the NP, in this case applying heat of 500 °C.(8) Furthermore, a magnetic NP can be added that enhances the interaction of the two compounds. On the other hand, a great catalyst that improves this interaction is the epoxy that can be added in the main chain of the PVP. (Figure 8c). The results with these reactions are NPs with a size of 7 nm and the amount of oxygen they present is half of 15.30 at% compared to the original NPs that are 33.45 at%. In this way, they can be used in biomedical applications.(8,37)

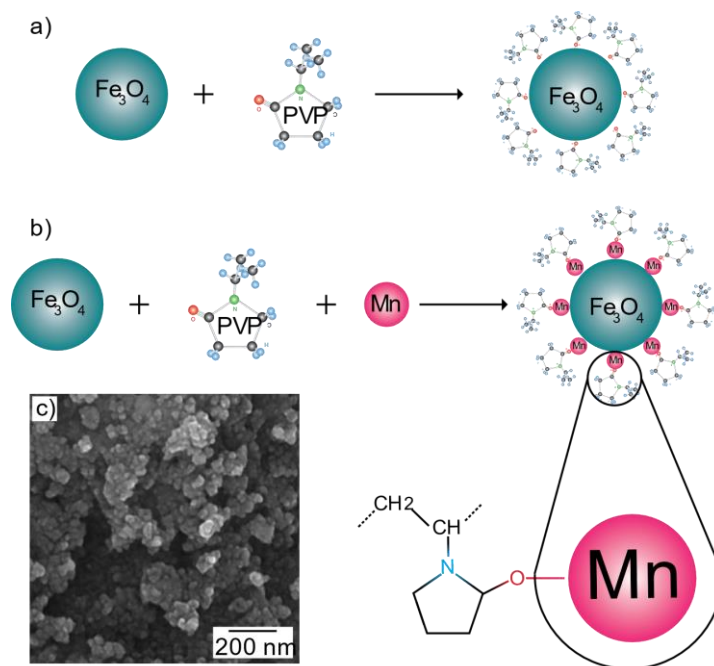


Figure 8. a) PVP coating process with Fe_3O_4 , b) Addition of epoxy to the PVP/ Fe_3O_4 functionalized particle, and c) TEM image of PVP/ Fe_3O_4 /epoxy biomedical particles. (adapted from *Organic Coatings Journal*) (37)

1.1.4.2. Pharmaceutical applications

Generally, in the field of pharmacology, PVP is used as an excipient or pill coating, since it helps control drug dosage. The most common medication is paracetamol, which is covered by PVP K-90 at 4%. (38) Hydroxypropyl methylcellulose (HPMC) is traditionally used as the main binder shell, but PVP proved to be much faster and more effective. These improved properties are due to

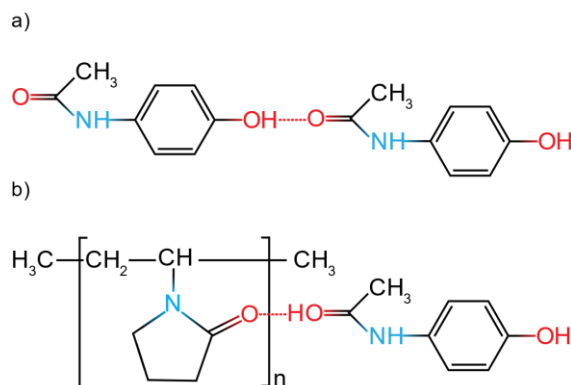


Figure 9. a) Hydrogen bonding between acetaminophen/acetaminophen and b) PVP/acetaminophen (adapted from *Organic Chemistry*). (38)

the fact that PVP has greater cohesion and adhesion work, especially with hydrophilic surfaces. In addition to being used as an excipient in addition to lactose-based Microcrystalline Cellulose (MCC), producing larger granules. (Fig.9) (33,38)

1.1.4.3. Industry applications

In the fields in which PVP stands out the most is in the industrial area, since it is easy to handle, highly versatile and adaptable. (35,39)It is essentially used as a scaffold for molecular structures, providing greater stability in the compounds that can be added. However, all these characteristics contribute mainly in the areas of adhesives, protective colloids, resin compounds, among others. (Table 3) (11,32)

1.1.4.4. Biomedical applications

In the biomedical area, PVP plays a very important role, since it has the characteristic, which allows its use in medicine, of not being toxic to life. Despite being a very effective bactericide and viricide suspected with Iodine, PVP/I or povidone-iodine, which was transmitted with great frequency in areas contaminated by the recent COVID-19 virus pandemic. (40) The pure state of PVP has low or no toxicity, which is highly compatible with life, including proliferating cell growth. (41)

The hydrogels application for medical use was sought in a polysaccharide known as carrageenan, one of the most abundant and therefore cheaper, was added to the PVP. (10)This polysaccharide has water-soluble sulfates with the ability to form thermoreversible gels. To link the carrageenan to the PVP, a radiation crosslinking process is used, linking the two carbons of the main chain to the carrageenan. (Fig. 10a)(10,42)

Photography	Adhesives	Protective Colloids	Resin Compounds	Films	Textiles / Fibers	Paper / Printing
photo emulsion additives	water-activated (envelopes, stamps)	particle-size regulators	dye-receptivity/printability improvers	printability improvers	dye stripping	strength improvers
colorant receptors	pressure-sensitive	suspending agents	compatibilizers for heterogeneous resins	adhesiveness improvers	dye-receptivity improvers	sizing agents
	glue sticks	viscosity modifiers	filler dispersants	anchor coatings	pigment dispersants	pigment dispersants
	bookbinding		wood plastic composites	anti-fogging agents	anti-fouling agents	ink removal in recycling paper
			anti-static agents	image receiving coatings	hydrophilicity improvers	ink jet paper
Coatings / Inks	Laundry Detergents	Metal Working	Oil / Gas Fields	Electrical	Ceramics	Cosmetic
pigment /dye dispersants	anti-redeposition agents	metal quench bath	drilling fluid additives	black matrix for TV tube	binders for green sheets	hair gel
viscosity modifiers	dye-transfer inhibitors		fluid loss control	binders for battery electrodes		hair spray
film levelers	binders for tablet formulations		gas hydrate preventors	nonwoven battery separator treatment		lip stick

Table 3. Different applications of PVC for the industrial area and its scope in everyday products. (32)

On the other hand, scientists with their great wisdom, not only saw that PVP could replace carboxymethyl cellulose (CMC); rather, by binding to PVP, it improves the mechanical properties and structure of both compounds, generating a porous mesh for cell growth. Figure 10b shows the schematic illustration of the structure of the hydrogels before and after phase separation. (10,41) Finally, figure 10c shows the basic structure of what is sought in hydrogels with PVP, showing the porous matrix. The purpose of this matrix is to isolate and protect each cell, while guiding growth in a controlled and orderly manner. Therefore, in studies carried out by scientists

Roy and Sha at Tomas Bata University in Zlin, they demonstrated the high capacity for cell proliferation in these hydrogels and their simple adhesion to the cell matrix.(10,40)

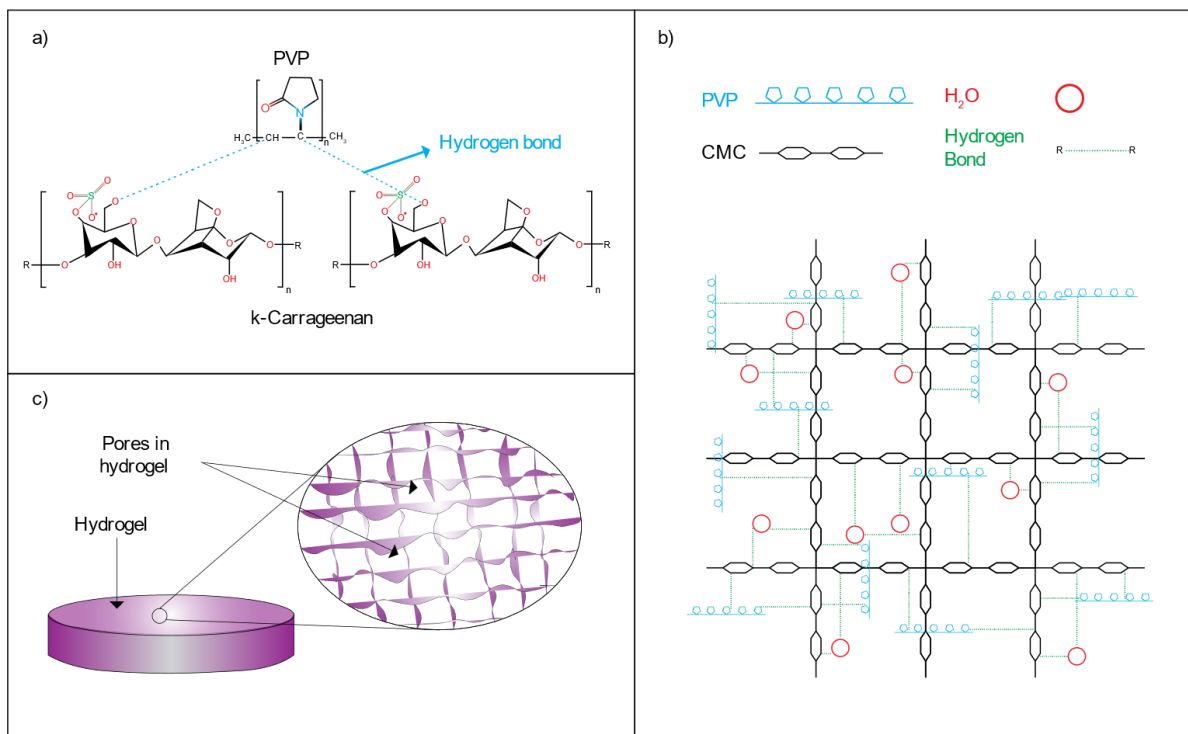


Figure 10. a) PVP- Carrageenan Blend Hydrogels, b) PVP- Carboxymethyl Cellulose (CMC) Blend Hydrogel and c) 3D crosslinked porous structure in hydrogel. (Adapted and modified from Internal Grant, Tomas Bata University in Zlin, Czech Republic) (10)

In vitro studies show the capacity of hydrogels for tissue regeneration in superficial lesions. The hydrophilic properties of these PVP hydrogels show a low interfacial tension, that is, they allow uniform migration and dispersion of cells through the porous matrix of the hydrogel.(10)

The application of hydrogels with PVP was used for the first time in burns by the doctor Rosiak in 1989, showing that it keeps the dressing moist, which helps faster treatment. These PVP/CMC hydrogels have properties such as: pain control, antibacterial barrier, easy handling, permeability, drug dose control, biocompatibility, among others. (Fig. 11a) (10,43)

Biocompatibility is a very important factor in hydrogels, as it prevents the body from rejecting cell regeneration. In addition, it reduces muscle contraction, in third degree burns, which usually requires total immobilization. To demonstrate this mechanism, Maher S.A. conducted a study of

biodegradable hydrogel implants in focal cartilage defects. For this, two PVP/PVA implants with modules of 0.6 MPa and 0.2 MPa are designed. The study concluded after 6 months, showing that the treated animals did not register death or intoxication due to the adhered implants. (Figure 11b)(10,44)

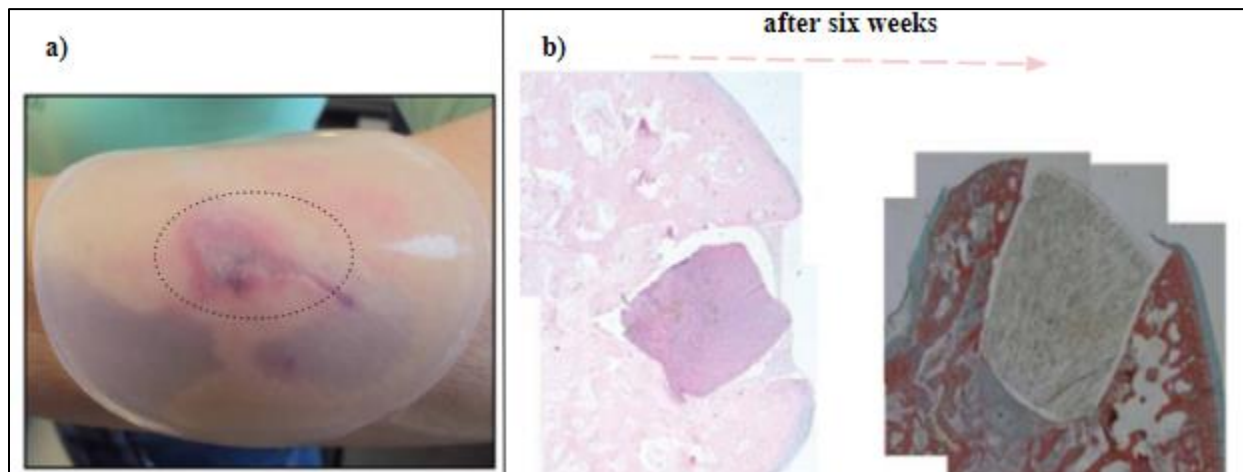


Figure 11. a) PVP-CMC hydrogel applied in moist heat treatment and b) microporous PVP/PVA scaffold for the repair of focal articular cartilage defects (Adapted and modified from Internal Grant, Tomas Bata University in Zlin, Czech Republic)(10,44)

1.2. Carbon-based materials

Carbon is the fourth most abundant element in the universe, after hydrogen, helium and oxygen, so its high capacity to react with various compounds, in addition to its morphological properties. (45)Carbon has an atomic mass of 12.01 and is a tetravalent nonmetal. The valence of these four electrons is determined in the 2s, 2p_x, 2p_y and 2p_z orbitals, so it can generate molecules from zero to three dimensions. For this reason, the number of molecular hybrid orbitals is three with sp² configuration (σ bond) in the same plane at 120° and a free orbital 2p_z (π bond) perpendicular to the plane of the three orbitals. (Fig. 12)(46–48)

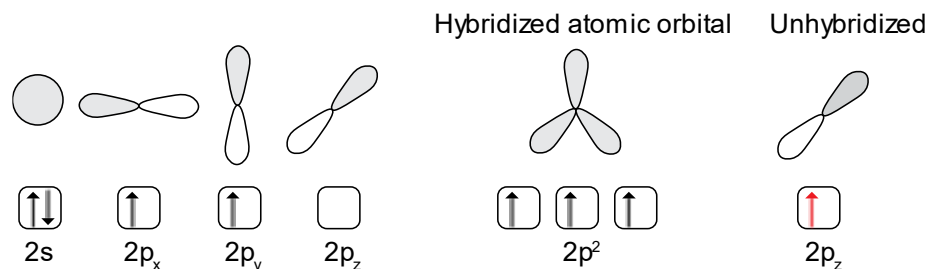


Figure 12. Molecular orbital theory applied in carbon atom. (adapted from *Organic Chemistry*) (49)

1.2.1. Atomic structure and morphology of carbon nanotubes

Carbon has several allotropes that can be configured from its configuration, such as: graphite, diamond, fullerene, amorphous carbons, carbon nanotubes (CNTs), and graphene. By placing the atoms in one plane or two dimensions, carbon generates hexagons (honeycomb lattice) that will have angles of 120° . This generated film of an atom thick is known as Graphene, and by taking this layer to the third dimension, rolling it up, a CNT can be obtained. (Fig. 13)(50–52)

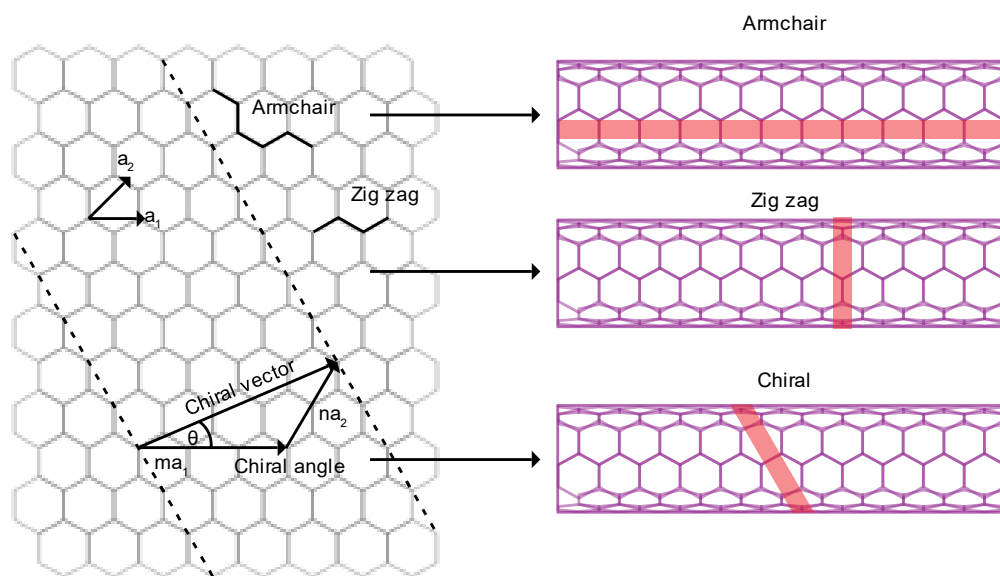


Figure 13. Construction of the graphene layer, layer curl, with the chiral vector and the angle. Also, it shows your Armchair and Zig-Zag shape and vector latitudes a_1 and a_2 . (adapted from *Composites Science and Technology and Physica E Low-dimensional Systems and Nanostructures*) (53)

There are three types of CNTs that can be obtained from the chiral indices n and m . The first, armchiral type, occurs when $m=n$ and angle is 30° , the bonds between carbons are perpendicular

to the CNT.(52,54,55) On the other hand, the zig-zag type is generated when the values of m or n are equal to 0 and angle is 30°, this indicates that the carbon bonds are parallel to the CNT axis. Finally, the chiral type appears when there is a mirror symmetry, that is, $n \neq m$ and angle is between 0 to 30 °. (Fig.13)(53)

Analyzing the electronic properties of CNTs, the indices n and m can tell us if it behaves like a metal or a semiconductor. In this way, the zig-zag type CNTs are metallic or semiconductor, and the armchair type are always metallic.(51,56) This CNTs properties could be confirmed by two propositions: if $|n - m = 3q|$ are metallic or those $|n - m = 3q \pm 1|$ are semiconductor.(57)

$$[3] \quad \mathbf{C}_h = m\mathbf{a}_1 + n\mathbf{a}_2$$

$$[4] \quad \theta = \arctan\left(\frac{\sqrt{3}m}{m+2n}\right)$$

$$[5] \quad d = \frac{C_h}{\pi} = a \cdot \sqrt{\frac{3(n^2+m^2+nm)}{\pi}}$$

Different types of CNTs can be obtained depending on their orientation defined by chiral vector \vec{C}_h and angle θ . The number of CNTs with addresses $\mathbf{a}_1 = \left(\frac{3}{2a}, \frac{\sqrt{3}}{2a}\right)$ and $\mathbf{a}_2 = \left(\frac{3}{2a}, -\frac{\sqrt{3}}{2a}\right)$ are denoted by the chiral values n and m. In this case a1 and a2 are the lattice vector that will indicate the winding direction [3,4]. Furthermore, the diameter of NTs and relationship between n and m, could be calculated with a, that is the length between carbons (1.42 Å) [5]. (57)

1.2.2. Multi-walled carbon nanotube

The diameter achieved by the CNTs varies between 0.4nm and 3nm. If it take several of these nanotubes and wind them one after the other, it will obtain the multi-walled carbon nanotube (MWCNT) with diameters and lengths of 100 nm and 9.7µm. respectively. Each CNT can be formed from graphene sheets with three types: cylindrically curved coaxial, polygonal coaxial or scroll graphene sheet. (48,50)

The average of the internal diameters of these layers varies between 5nm to 10nm, and the external diameter between 40nm to 60nm. In general, the cylindrical coaxial model is the most used for its stability and symmetry, despite this, it is possible to find polygonal coaxial shapes when they are

synthesized. (47) To accommodate this geometry, larger diameter tubes often allow three-dimensionally correlated regions, forming angles with low, aligned rake limits. (Figure 14)(45)

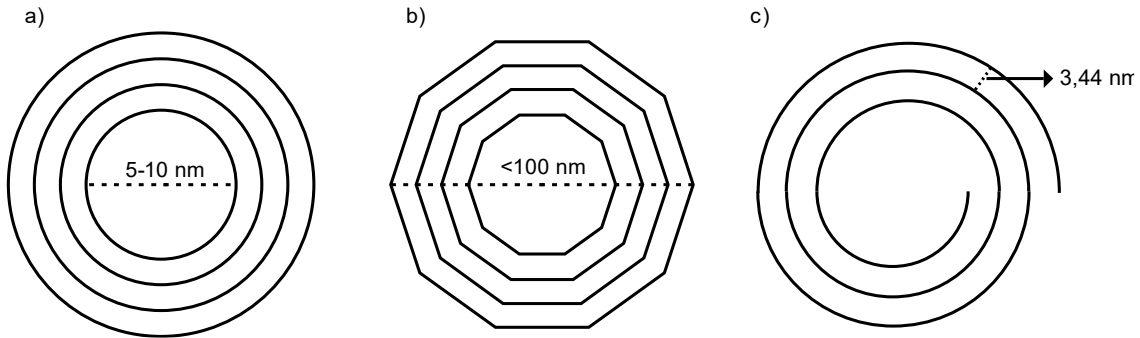


Figure 14. a) Cylindrically curved coaxial, b) polygonal coaxial and c) scroll graphene sheet. (adapted from Avenue du Recteur Pineau, Poitiers Cedex, France) (45)

The configuration of the MWCNTs only allows a sequence of n and m , where $n \neq m$, therefore the CNTs are of the chiral type, in order to maintain the distance between each layer. The average range of the distances between each layer of the MWCNTs is from 0.334 nm to 0.36 nm. In this way, the distance between each multiwall (MW) has a dependency on the size of the CNT. (48) For this, a value is generated that demonstrates in experimental data the radius of the tube ($\frac{c}{4\pi}$), causing the radius to drop to 0.344 nm [6]. When comparing the surface area of the CNTs and the MWCNTs, significant variations in their values are determined. A sheet of graphene shows a value of $1315 \frac{m^2}{g}$; on the other hand, when the MW is built the value decreases to $50 \frac{m^2}{g}$. (45,46)

[6]
$$d = 0.344 + 0.1xe^{(-\frac{c}{4\pi})}$$

Once these data have been analyzed, the main reason for the use of MWCNTs should be emphasized. To do so, Table 4 compares the main characteristics between SWCNTs and MWCNTs. In addition, its usefulness and malleability are taken into account, together with its synthesis, since as SWCNT is more delicate and simpler, its use is limited and its value increases. (48)

SWCNT	MWCNT
Single layer of graphene.	Multiple layers of graphene
Catalyst is required for synthesis.	Can be produced without catalyst.
Bulk synthesis is difficult as it requires proper control over growth and atmospheric condition.	Bulk synthesis is easy.
Not fully dispersed, and form bundled structures.	Homogeneously dispersed with no apparent bundled formation.
Resistivity usually in the range of 10^{-4} – $10^{-3} \Omega \cdot m$.	Resistivity usually in the range of 1.8×10^{-5} – $6.1 \times 10^{-5} \Omega \cdot m$
Purity is poor. Chemical vapor deposition (CVD) method is about 30–50 wt%. However high purity up to 80% has been reported by using arc discharge synthesis method.	Purity is high. Typical MWCNT content in as-prepared samples by CVD method is about 35–90 wt%.
A chance of defect is more during functionalization.	A chance of defect is less especially when synthesized by arc-discharged method.
Characterization and evaluation are easy.	It has very complex structure
It can be easily twisted and are more pliable.	It cannot be easily twisted.

Table 4. Difference between SWCNT and MWCNT. (adapted from Journal of Chemistry) (48)

1.2.3. MWCNTs synthesis

Currently, the demand for MWCNTs has increased since they need to cover more fields of application, such as medicine, physics, the automotive industry, among others. To meet this demand, scientists must solve four main problems that are mass production, selective production, organization and mechanism. There are three main techniques for manufacturing MWCNTs: arc discharge, laser ablation, and CVD. It also requires three main ingredients: a catalyst, a carbon source, and high amounts of energy. (51)

1.2.3.1. Arc-discharge method

As mentioned before, one of the fundamental elements for the production of MWCNTs is a rich source of carbon.(47) For the arc-discharge method, two electrodes made of pure graphite

(99.99%) are used, one bar with a diameter of 11 mm that acts as cathode and the second bar with a diameter of 9 mm that acts as anode. Also, for carbon, add to the atmosphere if you insert methane gas (CH_4) down one channel, and on the opposite side it has a vacuum pump to stabilize the reaction. A spectrophotometer is used which records the optical emission of the plasma (300nm to 650nm). Pressures ranging from 100 torr to 300 torr are often added, and the transmitted spectra are recorded for 300ms. It always has a cooling system to be able to control the exact temperature, since the plasma usually rises to 3000 °C. All the MWCNTs produced are collected at the cathode, so that they can be characterized by SEM or Raman spectroscopy. (Fig. 15)(48)

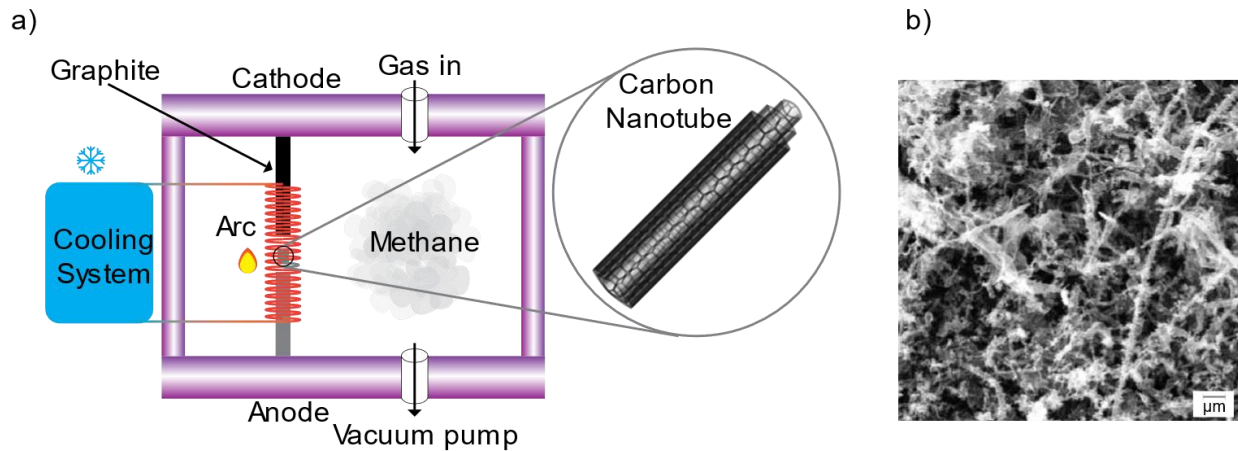


Figure 15. a) Arc-discharge Mechanism, b) MWCNTs SEM (L-band). (adapted from *Nanoscale Journal and Journal of Nanomaterials*)(47,48)

1.2.3.2. Chemical vapor deposition

CVD process uses an inert gas and hydrocarbon gas (for example, ethylene and acetylene) as the carbon source, which enter from the side of the reaction chamber and exit in a controlled manner(45). Once the gas enters, the chamber is heated in a range of 850 °C to 100 °C for the SWCNT and 505 °C to 700 °C for the MWCNT. The final discharge that is generated inside the chamber causes carbon to form from hydrocarbons, dissolving in metallic NPs. (Fig. 16) (51)

At this point, a maximum peak is generated where layers of semi-fullerene begin to be generated on the substrate. This semi-fullerene begins to extend in a cylindrical shape towards the top generating the MWCNT. In this situation, two scenarios can occur: base growth model of

MWCNTs growth mechanism or tip-growth model of MWCNTs growth mechanism. (Fig. 16)(46,51)

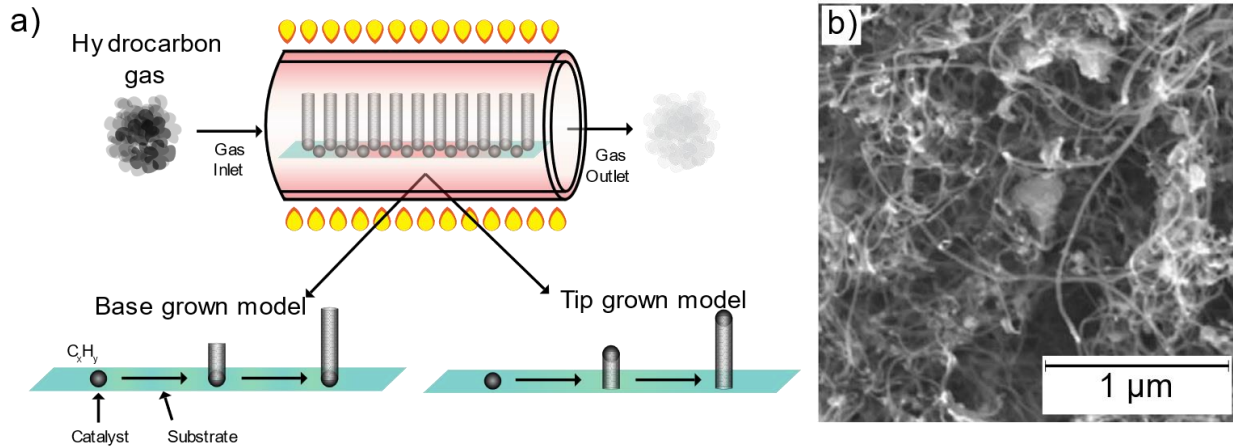


Figure 16. a) CVD mechanism, b) base growth model, c) tip-growth model and d) MWCNTs SEM image (adapted from *Chemical and Biological Technologies in agriculture and Applied Surface Science*)(46,51)

1.2.4. MWCNTs properties

The properties of hardness and tensile strength, MWCNTs have such wide applications in the field of science. The composition and morphology of MWCNTs make them one of the best carbon allotropes to use, as they have high conductance, interatomic strength, and excellent elasticity. It is also resistant but with the ability to absorb microscopic substances or molecules of water or gases. (58)An interesting part of the MWCNTs is Young's modulus, in the narrow non-orthogonal model, being approximately four times greater than that of diamond. The optimal amount of MWCNTs for high tensile strength is 50% and yield strength is 60%. (Table 5) (2,6)

MWCNTs properties	
Diameter	20-100 nm
Length	10-30 μm
Average interlayer distance	0,34 nm
Special surface area	90-350 $\frac{\text{m}^2}{\text{g}}$
Bulk density	0,05-0,17 $\frac{\text{g}}{\text{m}^3}$
Electrical resistivity	2×10^{-3} to 1×10^{-4} $\Omega \cdot \text{cm}$
Volume resistivity	0,1-0,15 $\Omega \cdot \text{cm}$
Electrical conductivity	11×10^5 $\frac{\text{S}}{\text{m}}$
Aspect ratio	100-1000
Tensile strength	10-60 Gpa
Tensile modulus	1000 GPa
Thermal conductivity	3000-6000 $\frac{\text{W}}{\text{m} \cdot \text{K}}$

Table 5. MWCNTs physics properties (1,2,58)

1.2.5. MWCNTs SEM and Raman spectroscopy

In the Raman spectrum of MWCNTs, the following are observed: the G-band and the D-band. The G-band is commonly applied for the determination of CNTs. This band is usually associated with an increase in defect density. (1,2)The G band can be associated with the degree of crystallinity of the CNTs, and its intensity is proportional to the crystallinity of the sample. In the case studied, the high degree of symmetry and the ordered structure of the carbon materials give rise to a graphite band (G band) in the region of $1550\text{-}1600 \text{ cm}^{-1}$. The other is the broad top of D-band between 1385 and 1399 cm^{-1} . Peak D indicates the presence of defects in the graphite material. The relationship between the intensity of the D band and the G band (I_D/I_G) is an important feature of extended defects in CNT structures. (Fig.17a)(59,60)

Raman spectra of aMWCNT and fMWCNT are shown in figure 17b. For both samples, two peaks occur around 1330 cm^{-1} (D band) and 1580 cm^{-1} (G band). The D band corresponds to sp^3 -hybridized or disordered carbons in the wall of CNTs, and the G band is attributed to oscillations of sp^2 -bonded carbons in graphene-like structures such as CNTs. This result indicates that the oxidants do not destroy the graphite structure of the CNTs because the peaks do not change after oxidation. The increase in the intensity of the D band was found to be an indication of $\text{sp}^2 \rightarrow \text{sp}^3$ hybridization from covalent binding of different functionalizes. (Fig. 17b)(59,61,62)

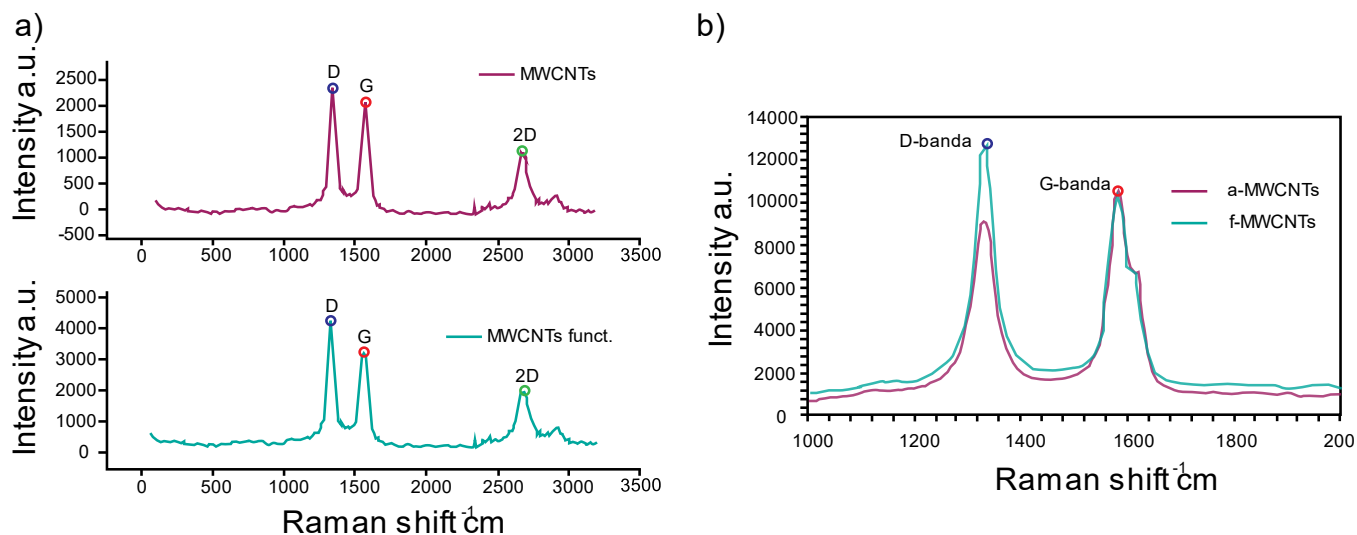


Figure 17. a) shows the MAWCNTs Raman spectroscopy non-functionalize and functionalized and b) shows the MWCNTs Raman spectroscopy for aMWCNT and fMWCNT. (adapted from *Organic Chemistry*) (32)

The structural and surface morphology of the MWCNT samples was evaluated by SEM. Figure 18 shows the SEM images of pristine MWCNTs at the 500nm magnification scale. It shows that the pristine MWCNT has a smooth surface with tangled tube bundles. However, it is clear from figure 18 that pristine MWCNTs contain many impurities on their surface. There was no presence of trace impurities in both MWCNTs due to oxidation during acid treatment. SEM observations show that MWCNTs have less structural damage on their surface. (59,60)

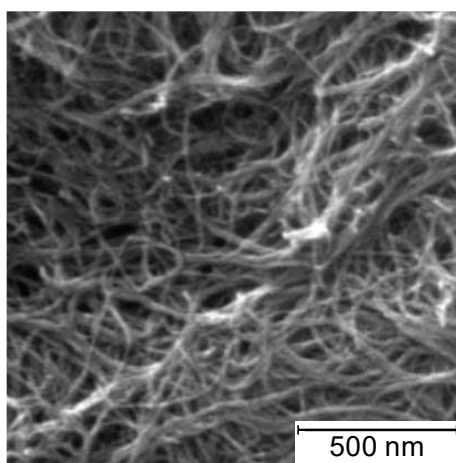


Figure 18. Image from MWCNTs fibers. (adapted from *Journal of Chemical Engineering & Process Technology*)

(41)

1.2.5. MWCNTs applications

1.2.5.1. Artificial muscles with MWCNT/PEDOT

The biological alloy with the inorganic has been sought for a long time in order to improve the human being. There is an experiment that has tried to generate a hybrid muscle that has the muscle cells with the artificial structure.(4,61) The most difficult problem to solve is the compatibility of the cells with the scaffold on which the hybrid muscle is built. The use of sheets of MWCNTs coated with poly (3,4-ethylenedioxythiophene) (PEDOT), it was possible to generate adequate biomimetics. This is regulated from electrical fields that generate a small contraction movement. (Fig. 19)(63)

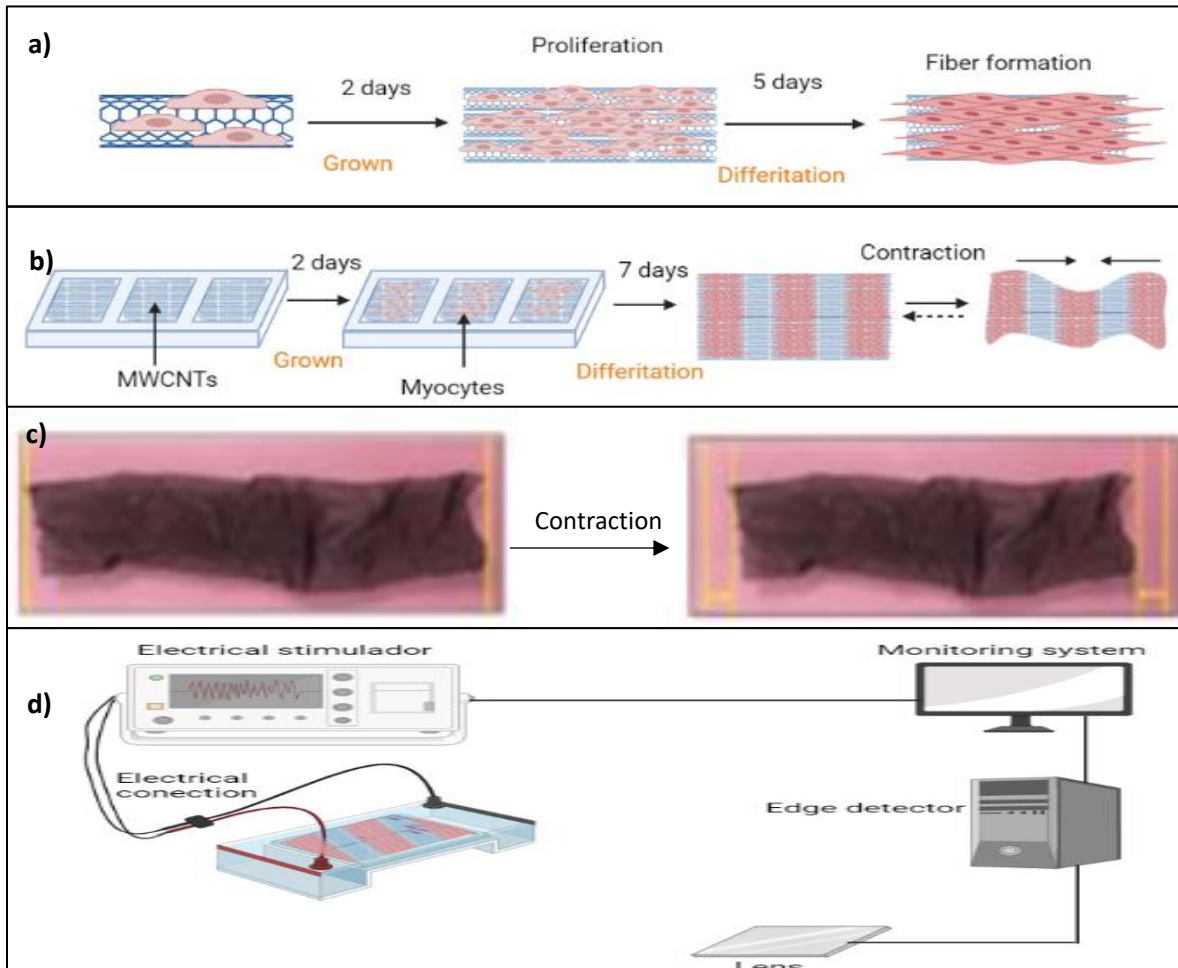


Figure 19. a) Proces of cell proliferation in MWCNT/PEDOT matrix, growth after 2 days and differentiation after 5 days, b) matatrix parts and scheme of muscle contraction, after 7 days the muscl n can contract, c) muscle contraction in vitro and d) control of cel prolifertaion in MWCNT/PEDOT with electric stimulation. (ataped from Scientific Report)(63)

1.2.5.2. MWCNT/CS to develop 3D scaffolds for nervous tissue repair

In injuries that are generated in nervous tissue, the difficult part is not regeneration, the complex part is the adequate rehabilitation of each nerve, that is, that they follow the appropriate path of regeneration. The small amount and complexity of nervous tissue makes their treatments highly expensive. To construct a suitable scaffold, chondroitin sulfate (CS) was used with MWCNTs for the regulation of neuronal growth. A self-assembly technique was performed by cultivating neuronal progenitor cells, obtaining a culture duration of 20 days. Viable repair is possible if MWCNT/CS scaffolds are applied in the acute phase. To stimulate the formation of fibroglial scarring, guaranteeing longer neuronal activity. (Fig. 20)(57)

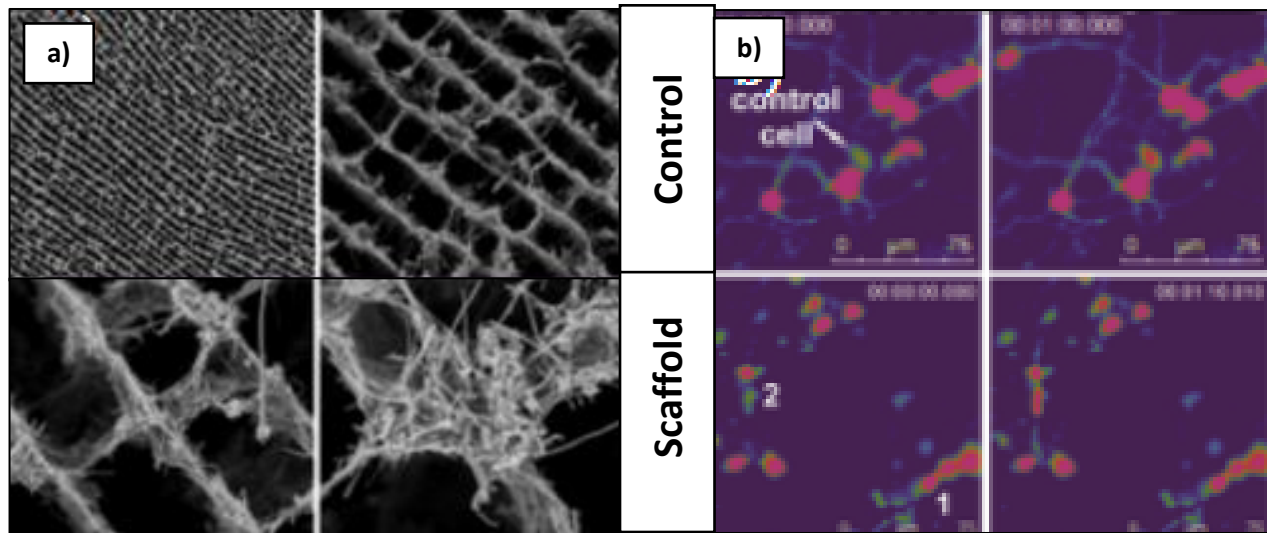


Figure 20. a) SEM image of CS/MWCNT scaffolds from 200 μm to 5 μm and b) To obtain cell proliferation, Fluo-4 was applied, which stains the cells to be observed; control was performed in glass and the test in MWCNTs/CS. The fluctuation of fluorescence that is obtained is plotted against time; also, four specific cells were labeled to compare their proliferation activity. (adapted from Biomaterials)(57)

1.3.MWCNTs/PVP

The synthesis of novel PVP/MWCNT composite nano-fibers by the electrospinning process is reported. Some possible wrapping arrangements of PVP on a CNT. Backbone bond rotations can induce switch-backs, allowing multiple parallel wrapping strands to come from the same polymer chain. (Fig 21)

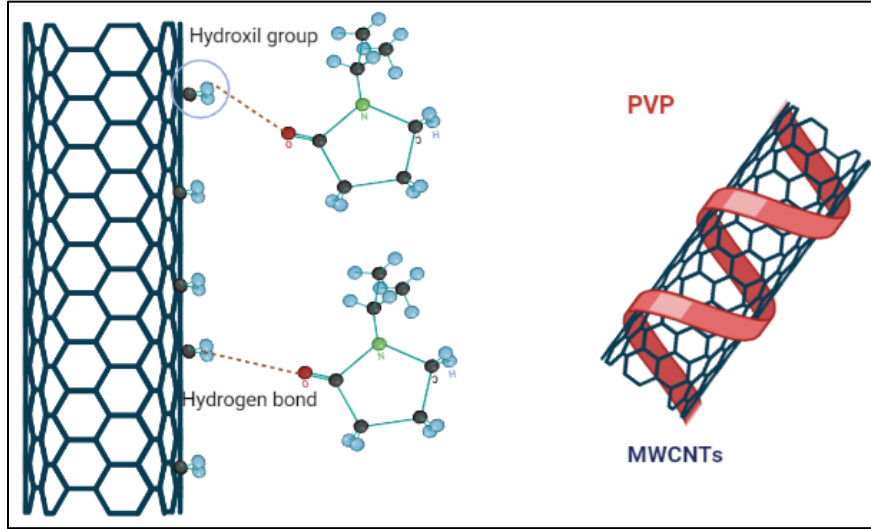


Figure 21. Show bond between hydroxyl group from MWCNT with oxygen from PVP and morphological binding of PVP on MWCNTs.

The wet membrane was then weighed wiping the water from its surfaces. Subsequently placed in an air-circulating oven at 50 °C until its weight stabilized. The weight of the dry membrane was recorded and its porosity was calculated using the following equation [7]:

$$[7] \quad \varepsilon = \frac{W_w - W_d}{A \cdot l \cdot \rho} \cdot 100\%$$

where ε is the membrane porosity, W_w and W_d are respectively the weights of the wet and dry membranes, A is the effective area of the membrane (cm^2), l is the membrane thickness (cm), and ρ is the density of pure water ($\frac{g}{cm^3}$)(52)

Pore radius (r_m) was determined by the Guerout–Elford–Ferry equation on the basis of the pure water flux and porosity data [8]:

$$[8] \quad r_m = \sqrt{\frac{(2.9 - 1.75\varepsilon)8\eta l Q}{\varepsilon \cdot A \cdot \Delta P}}$$

Where η is the water viscosity (8.9×10^{-4} Pa.s), Q is the volume of permeate pure water per unit time ($\frac{m^3}{s}$) and ΔP is the operation pressure (0.1 MPa).(64)

1.3.1. MWCNTs/PVP Synthesis

The considered possible model of PVP-assisted CNC self-assembly assumes that adsorbed PVP molecules block lateral bonds between CNC particles and promote said self-assembly. Due to the amphiphilic nature, PVP can affect the morphology and growth of nanoparticles by ensuring their solubility in various solvents, discriminating surface determination, controlled crystal growth, playing the role of a shape control agent, and facilitating growth. of specific crystal faces while preventing others. (Fig. 22)(52,65)

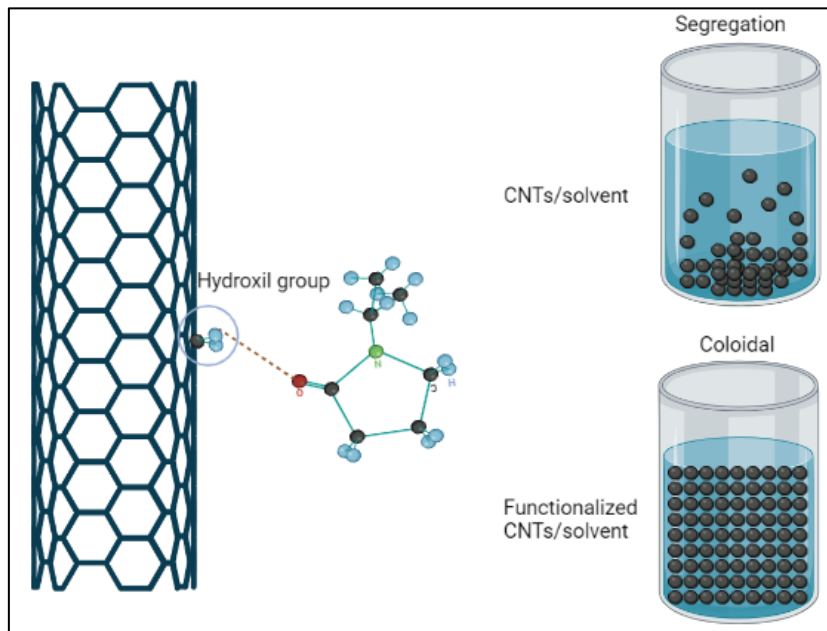


Figure 22. In the image is possible distinguish the hydrogen bond, that was functionalized, in contrast with solvent dispersion on CNTs.(6)

A stable aqueous MWCNT dispersion was obtained by using non-ionic surfactant PVP with the optimized PVP/MWCNT weight ratio of 20% from the above dispersions investigated. MWCNT/PVA hydrogel preparation. The MWCNT–PVP dispersion was sonicated for 15 min at room temperature. Then PVA powder was added into the uniform MWCNT–PVP dispersion, and the mixture was stirred and heated up to 120 C in a YX-280 pressure steam sterilizer and maintained at 120 C for 1.5 h. With this method the result of amount of carbon, oxygen and nitrogen are 83.27% , 10.61% and 6.12% respectively. (Fig. 23)(7,54)

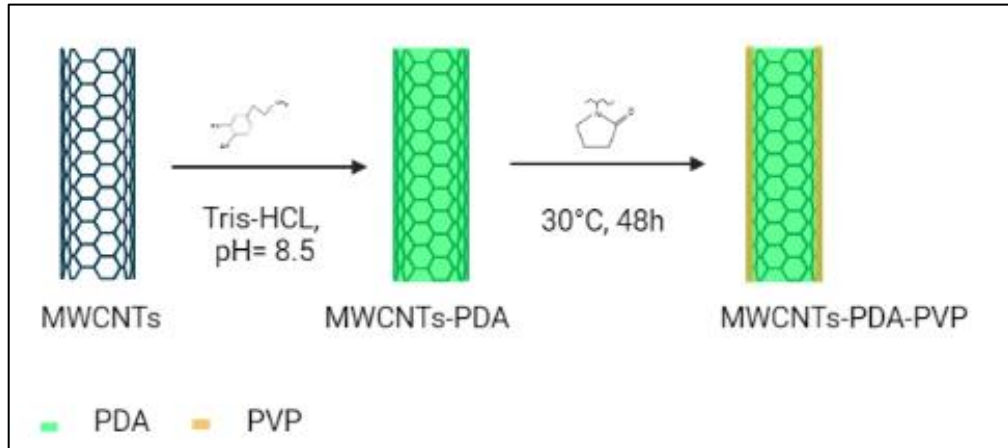


Figure 23. Process to inch the PVP on MWCNTS, it is use Tris-HCL with 8,5 pH, and the it heated by 48h at 30 °C(66)

1.3.2. MWCNTs/PVP properties

In the recent years, most studies have been focused on CNT/PVA composites in the form of fiber, film and bulk materials have achieved a 79% improvement in the tensile modulus and 47% improvement in the tensile yield strength for PVA films by the addition of 0.8 wt% of functionalized single-walled carbon nanotubes have obtained an increase by 160% in tensile Young's modulus with 5 wt% multi-walled carbon nanotubes in PVA matrix. A systematical study on carbon nanotubes reinforced PVA in hydrogel form in order to explore its full potential as multifunctional biomaterial has yet to be done. Carbon nanotubes are bound to form bundles, entanglements and agglomerates because of their intrinsic van der Waal interaction between tubes, which results in the insolubility or poor dispersity of carbon nanotubes in most organic and aqueous solvents and polymer matrices. Such agglomerates lower the contribution of carbon nanotubes as reinforcement in composites.(59)

Covalent functionalization of nanotube surface is an effective way of dispersing nanotubes. Single walled nanotubes can be dissolved in superacid, chlorosulfonic acid through direct protonation. However, covalent sidewall chemistry often induces substantial and/or irreversible changes to the structure and properties of nanotubes. (39)

During the dispersion process, an additional ultrasonication treatment of aqueous dispersions may help to nanotubes by providing high local shear, separating the bundles or agglomerates into individual nanotubes. PVP was selected to facilitate MWCNTs to disperse uniformly into PVA

hydrogel network so as to preserve pristine surface structure and exceptional mechanical and physical properties of the nanotubes.

1.3.3. MWCNTs/PVP applications

1.3.3.1. Physic industry

It is comprehensively investigated the interface between the PVP-coated silver nanoelectrode and the PVP-coated MWCNT to better understand the leverage of the PVP protective layer on the electrical performance and joining strength properties during the self-soldering process. This self-soldering process is performed within an environmental scanning electron microscope by a nanorobot-assisted nanomanipulation system.

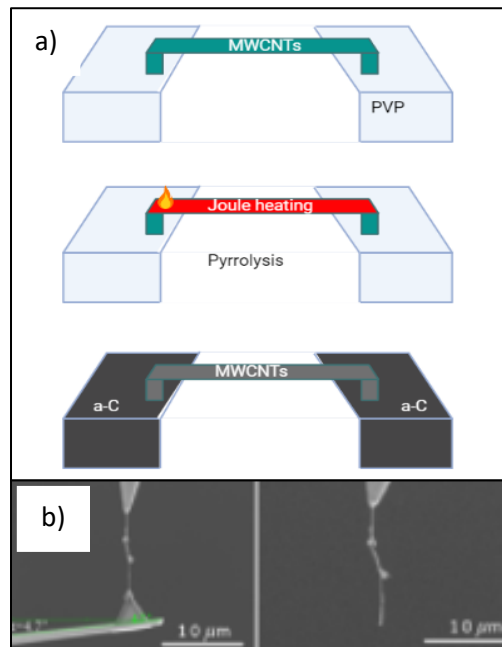


Figure 24. a) the heating mechanism of the MWCNTs with the PVP layers acting as support, b) load distribution system to send current to the MWCNTs and c) nanofiber MWCNTs with different steps. (adapted from *Applied materials and interfaces*)(39)

The results show that the conductivity of the soldered nanostructure is enhanced by about 1000 times after a 65 s vacuum annealing process. The PVP protective layer and the subsequently formed amorphous carbon layer from the PVP pyrolysis provide good antioxidant protection for the whole soldering process. The PVP-coated silver nanoelectrode was also successfully positioned and soldered onto the silver pad, which verifies the feasibility of the provided self-

soldering method. The recipe highlights the promise of soldering dielectric-coated electrodes for fabricating nanoelectronics devices and transparent conductive films. (Fig. 24)(39)

1.3.3.2. Biomedical application

The interaction of the cells with the substrates begins with the attachment of the cells to the surface of the material through the contact sites. The cells then strongly interact with the surface, which is essential for their communication and subsequent tissue formation. Therefore, we have used SEM images on fixed osteosarcoma cells and fibroblasts at 48 h to compare their morphology in all polymer-composite coatings formed.

It was not possible did not observe any morphological change of cells cultured in composites with an aggregate of MWCNTs compared to cells cultured only in pure polymeric coatings, indicating that the aggregate of MWCNTs does not influence cell morphology. At low concentrations of MWNCT, the PVP in PVP-based coatings can dissolve into the cell medium during the fixation procedure, leaving patches of undissolved polymer and densely packed cells around them. Finally, the biomedical application of the matrix would be used in in vitro detection in case of binding of proteins or biomolecules. (Fig. 25)(56)

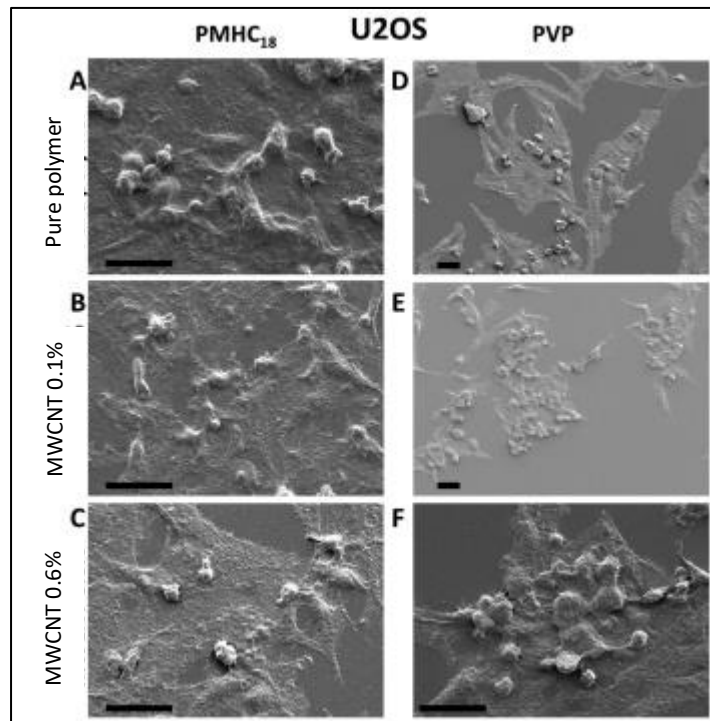


Figure 25. SEM image of MWCNTs with different concentration (0,6% and 0,1) with PVP (adapted from *Surface and Coating Technology*)(56)

On the other hand, it is also used for the detection of proteins from intestinal epithelial cultures, by exposure of the MWCNTs/PVP. Colloidal stability in culture medium, when plotted against the overall effect of f-CNT on protein expression, suggests that the less stable MWCNT-COOH had the greatest effect, while the more stable SWCNT-COOH had the least. effect in this exhibition. The comparative behavior of MWCNT-COOH and MWCNT-PVP confirms our previous observations about their stability in aqueous dispersions. (Fig. 26)(58)

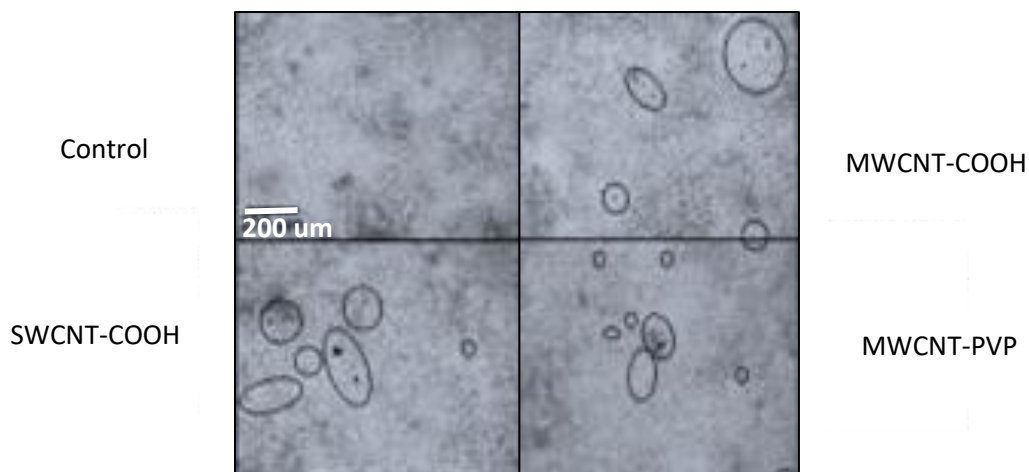


Figure 26. Analysis of proliferation in different matrix: control, SWCNT-COOH, MWCNT-COOH and MWCNT-PVP. (adapted from *Biomed Nanosci Nanotechnol*)(58)

CNTs are also used as support or scaffolds in biological structures, in the field of tissue engineering, to improve their deterioration. Despite this great freeze, neurons continue to be a field with difficult development in this environment. It is possible to generate a violation in the NTs and analyze them in scanning microscopy. A specific area is the cerebral ganglion, where it was incubated in a medium of MWCNTs/PVP at 4%. With computerized microscopy studies, its adhesion to the cells was increased, reaching the cytoplasm, thus crossing the cell membrane. (Fig. 27)(59)

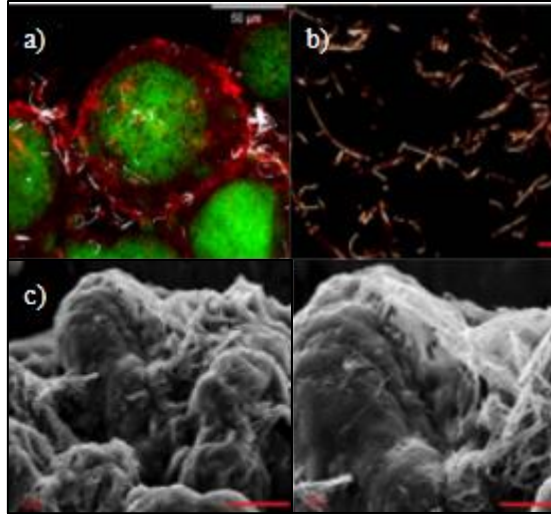
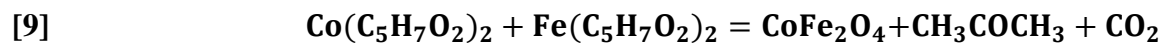


Figure 27. a) Grown of neuronal cells in MWCNTs/PVP, b) snail ringer in MWCNT where solution poise on glass and c) SEM to Analise MWCNT topography. (adapted form Sientific Research Publishing) (59)

1.4.NP and solvent

1.4.1. CoFe₂O₄ NP

Spinel ferrite magnetic nanoparticles have attracted great interest because of their unusual physical properties and their practical applications in several fields. Recently, a sol-gel auto-combustion method has been proposed for ferrite synthesis, and it possible to applied it to the preparation of cobalt ferrite, CoFe₂O₄.(69) In this method, precursor gels are prepared from aqueous solutions of metal nitrates and an organic material. Moving along these lines, it has already shown that the mentioned sol-gel auto-combustion method can be adapted to synthesize cobalt ferrite-silica nanocomposites, as shows next reaction [9](70):



In a flask with three necks, it is added under nitrogen flow and the rest of the materials are added: acetylacetonate cobalt (II) acetylacetonate Co(acac)₃, iron (III) acetylacetonate Fe (acac)₃, 1,2-hexadecanediol, oleic acid, oleylamine, and benzyl ether. The mixture is stirred and degassed at room temperature for 60 min; stop, then heat the mixture at 100 °C for 30 min. The temperature is then increased twice more to 200 °C and 300 °C for 30 and 60 min, respectively.(71) Finally the mixture is cooled to room temperature and purified three times with ethanol and hexane. The results of this synthesis give COF NPs with sizes from 6 nm to 16 nm. the size distribution with

an average diameter is obtained on a limited number of particles around 550 NPs. The size of the NPs increases if the duration of the heat treatment is increased. (Fig. 28)(72,73)

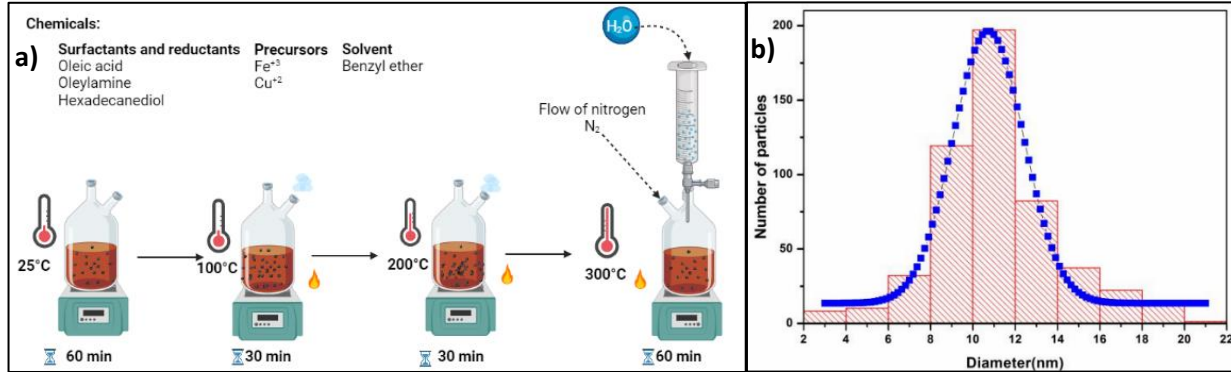


Figure 28. a) process of thermal decomposition method and b) dispersion of nanoparticles and their average diameter .(adapted from Scientific Research Publishing)

The critical diameter d_c from which the particle can be considered as a magnetic monodomain is defined by Frey et al. [10]:

$$d_c = \frac{36\sqrt{AK_{eff}}}{M_s^2\mu_0}$$

[10]

Where K_{eff} is the effective anisotropy and A is the exchange constant. μ_0 is the vacuum permeability and M_s is the saturation magnetization. d_c is in the range of 10-100 nm

CoFe₂O₄ (COF) NPs will be used to observe the dispersion of the MWCNTs with PVP based on the size of the NP. Different sizes of COF NP can be achieved, depending on the synthesis performed. The size that will be obtained from the NP will generate two possible results when analyzing the sample: the NP will generate dispersion in the polymer, or the NP will aggregate in the polymer. (Fig. 29)(12,74)

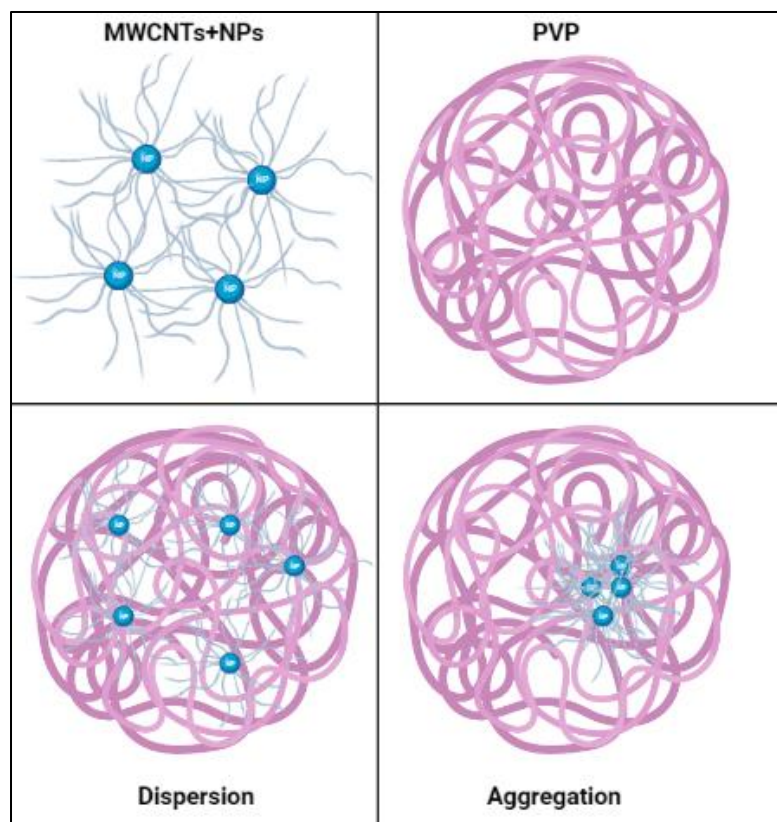


Figure 29. When aggregate the NPs at the MWCNTs/PVP could be happen these two situations: dispersion or aggregation (adapted from Chem Laboratories)(6)

1.4.1.1. COF SEM image and Raman spectroscopy

The Raman spectra seen four wavelength at 296, 465, 600 and 660 cm^{-1} , which are all characteristic of CoFe_2O_4 . Raman evidence was observed for common impurity phases such as Co_3O_4 and $\alpha\text{-Fe}_2\text{O}_3$, which indicated that a phase pure material had been fabricated in the bulk. (72,73)

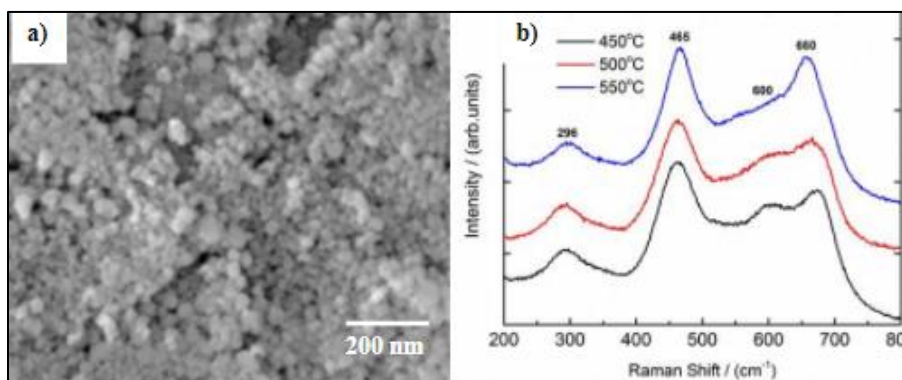


Figure 30. a) SEM image and b) Raman spectrum of COF NP. (adapted from Biomed Nanosci Nanotechnol)(71)

1.4.2. N,N-dimethylformamida and ethanol

The N,N-dimethylformamide (DMF) and ethanol are the compounds that will act as solvents for the process of synthesis and functionalization of PVP and MWCNTs. DMF is made up of the formula $(\text{CH}_3)_2\text{N-CHO}$, it is organic, liquid and miscible in water. Its application is directly in polymers since it is capable of generating hydrogen bridges and dissolving polymer chains. The objective is to be able to functionalize the PVP so that it is compatible with the MWCNT. (71,75) On the other hand, ethanol will be used as a solvent for PVP powder, it is also miscible in water, liquid and colorless. Its formula is $\text{C}_2\text{H}_6\text{O}$, its advantage is that it does not instantly break down any polymers, it only dilutes them. (Fig 31)(11,20)

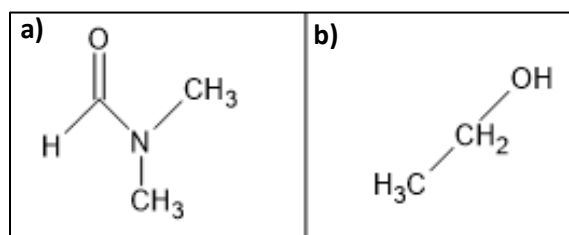


Figure 31. a) DMF and b) ethanol molecules. (adapted from Organic Chemistry)(25)

1.4.2.1. DMF and ethanol with PVP

In general, concentration is a primary factor determining the solution viscosity, whereas the value of surface tension depends on both the polymer and solvent. In this article, it report our investigation on the solvent effect on PVP nanofibers.(25) By adjusting the nature and compositions of solvents, solvent mixtures, and solution concentrations, it found that at the concentration of 4% by weight , a mixture of ethanol and DMF with a mass ratio of 50/50 was the best solvent system for obtaining ultrafine PVP nanofiber with an average diameter of 20 nm and a uniform size distribution. (Fig 32)(10,20)

Typically, the thin-film morphology consists of nanoparticles less than 100 nm that combine to form larger dendrites derived from the fluorine-doped SnO₂ (FTO) substrate. The largest dendrites were between 0.5 and 1 mm in diameter and evenly distributed over the substrate, the desired highly porous structure for supercapacitor electrodes. Electrodes with very porous dendritic structure have been reported for other materials such as Fe₂O₃ and ZnFe₂O using the CVD technique. The SEM image of the cross section can be seen in Fig. 32 in additional information.(3,8)

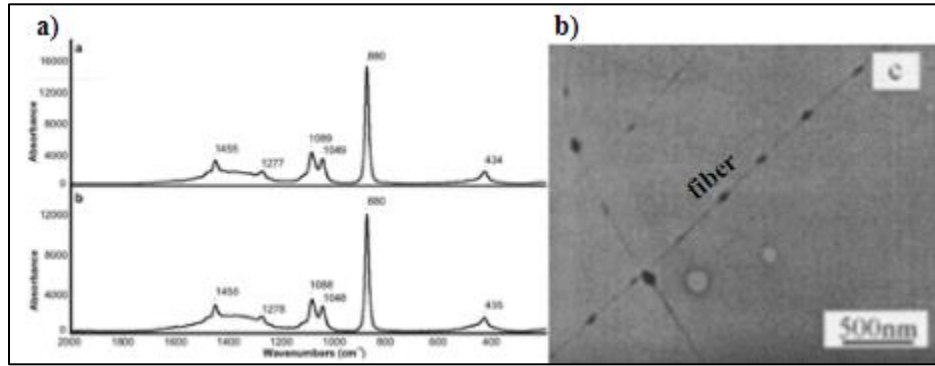


Figure 32. Raman spectrum and SEM image of PVP diluted in DMF and ethanol. (adapted from *Fisics Research Journal*)(8)

The appearance of the hollow core beads from the PVP/MC solution could be attributed to its low boiling temperature that causes a faster evaporation of the solvent from the surface of the polymer solution jet than that from the core of the fiber during electrospinning. They considered that the pressure, which was created by solution surface tension in the fiber, forced the solution into the beads, when excess charges on the fiber surface were neutralized by airborne ions created by the corona discharge. (table 6)(9,22)

System	Surface tension (cPs)	Viscosity (cPs)
Ethanol	29.3	17.3
DMF	47.1	9.8

Table 6. Properties of ethanol and DMT

Chapter 2

2. Motivation

Graphene took an extraordinary turn in the field of health, since the applications that were found from its discovery are practically endless. In the medical industry, graphene has been applied in implants, drugs, biomedical devices, among others. One of the derivatives is the MWCNTs that have also found their utility in health and biomedicine, for example it has been used for the covers of pills or the use of glucometer sensors. They are very useful since they have resistance, high hardness, flexibility and elasticity. On the other hand, it has polymers that are also very useful in the medical field, one of these is PVP. This polymer has several characteristics, among which it

stands out for medical use is its biodegradability and low toxicity. This is why PVP has been applied in hydrogels for skin regeneration or in surgical implants.

The alloy not only greatly improves the physical characteristics, but the human body better the PVP/MWCNTs. When the PVP binds to the MWCNTs, it surrounds the final nanotube generating a layer to the outside through a covalent bond between the hydroxyl oxygen and the free oxygen of the MWCNTs. Those bonds with high energy give better stability between the two compounds; it is for this reason that they are optimal for their characterization. Among other characteristics, it presents a conductivity, tensile strength and elongation at break greater than the two compounds separately, although the flexibility is relatively less than that of PVP, it is still viable for its biomechanical applications.

The main objective of the project is to synthesize and characterize a compound of PVP/MWCNTs, to analyze its optical, chemical and mechanical properties. In addition, in the medical field it is study the biocompatibility and durability within living organisms. This will be achieved based on analyzes performed in SEM, XPS and Raman spectroscopy.

2.1.Problem statement

PVP can be found in various devices that help the industry, but its properties can be mechanically improved with the application of MWCNTs. For this, there is some research that has shown the high degree of performance obtained with these two compounds. On the other hand, it find COF, which greatly helped its dispersion but has been little studied for its applications.

2.2.General and specific objectives

Characterize with Raman spectroscopy and SEM the mechanical properties of the PVP/MWCNTs-COF compound, with different sizes of the NPs.

Analyze the possible medical and biomedical applications of the compound based on its characterizations.

Chapter 3

3. Methodology

3.1. Optical microscopy

This type of microscope helps produce images by using a beam of electrons focused on the surface that needs to be observed. The topographic information that is obtained is given from the interaction between the electrons and the sample, in this way it emits a second electron beam that the SEM detects as see in. It is detecting these electrons; they generate an image with a range greater than 1 nm.(76)

3.1.1. Fundamental principle of SEM

The fundamental principle of SEM measurement is in the electrons emitted by a tungsten cathode, which will generate three different interactions: secondary electron, Backscattered electrons and Auger electrons. Of these, the main one is the secondary electron that can be detected. This electron, upon penetrating the atom, loses energy and will be distributed at different angles. (Fig. 33) (45,77)

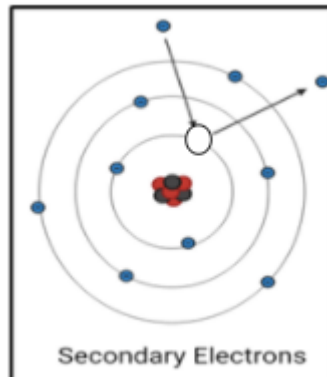


Figure 33. Secondary electron process for SEM. (adapted from Physics Studio)

3.1.2. SEM process

The parts of the SEM to measure these interactions is the electron emitting source, the secondary electron detector, a magnetic lens system, the image processing system, the scanning coils, the backscattered electron detector and the visual cathode ray tube and recorders.(76,77)

By using a thermodynamic process, the electrons that are emitted exceed the function of the work force. To accelerate the electrons, the lattice surrounds the filament, generating a negative polarization that causes the electrons to converge at a crossover point as they pass through the cathode. The utility of magnetic lenses is to condense the image and, in turn, condense and demagnetize the electrons. To avoid any external interference, the column from the cathode to the surface must be placed under vacuum.(76)

Among the different characteristics that are required to obtain an adequate image, applied voltage and high quality are: aperture size, current, lenses in good condition and clean sample. For the production of the image, a current density is generated that comes from the increase in voltage and the heating of the filament. (Fig. 34)(78)

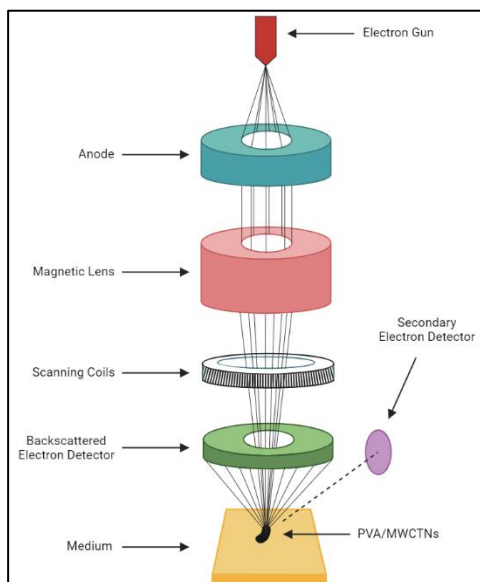


Figure 34. SEM device, principle and detents process to obtain de image.

3.2. Raman Spectroscopy

Unlike XPS and SEM, Raman spectroscopy analyzes the interaction of magnetic waves generated by atoms. For this analysis based on light scattering, a wavelength is sent and then the wavelength back is analyzed and data on the bonds between atoms is obtained. (79)

3.2.1. Fundamental principle of Raman

There are three types of dispersion that can be obtained: Rayleigh, where an elastic dispersion occurs, Stokes and anti-Stokes, in this case anti-elastic dispersions occur. These inelastic scatters generate Raman scattering, where the photons annihilate and create the scattering photon to be measured. For anti-Stokes scattering the transition is low, that is, the incident wavelength is greater than the emitted wavelength. In the case of Stokes scattering, the transition is high, which means that the incident wavelength will be less than the emitted wavelength. (Fig. 35)(80)

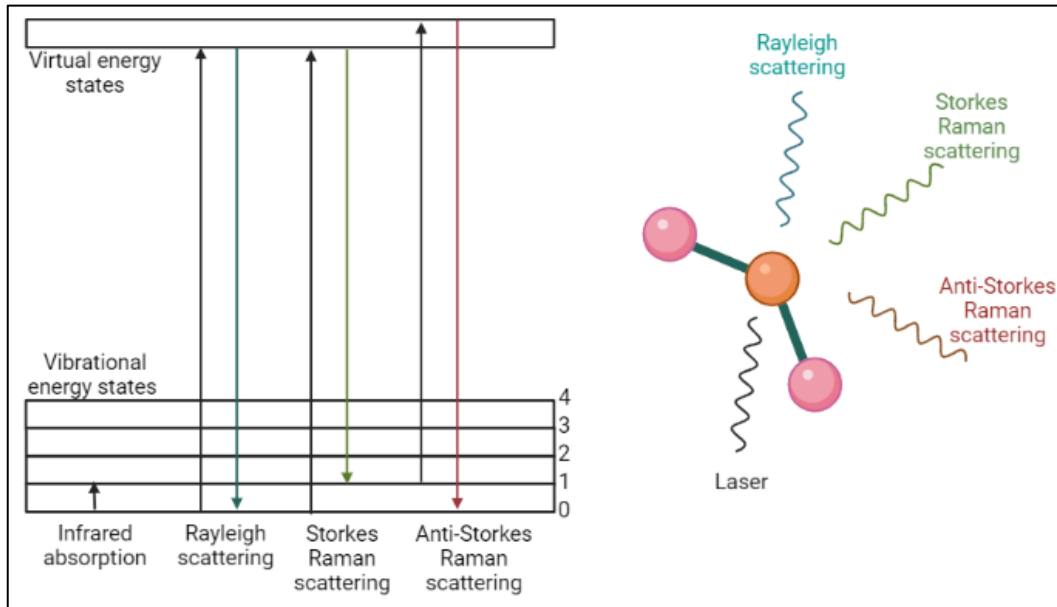


Figure 35. These vibration differences between each link will produce different changes in the photon frequency, which will help determine the properties of the material and three different reaction of fundamental Raman principle. (adapted from *Physics of Materials Journal*)(80)

3.2.2. Raman spectroscopy process

The process of generating an analysis with Raman spectroscopy involves inserting a beam of light into the acquisition field without a varied flow change, aiming to highlight molecular vibration. Additionally, it receives signals from the molecules and generates different processed images and data for study based on the value of the generated intensity.

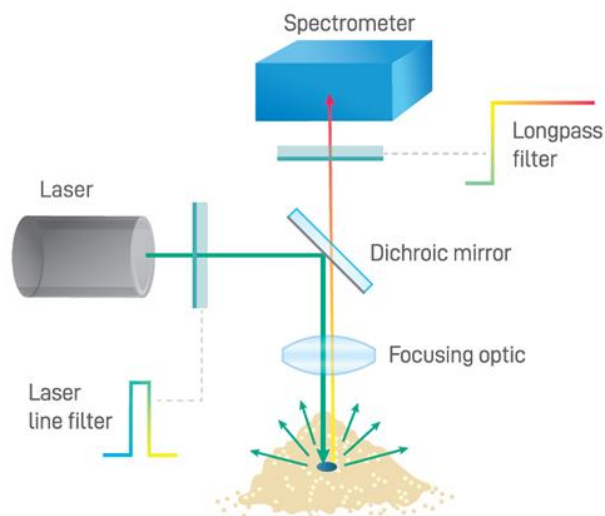


Figure 36. Raman spectroscopy device, each parts process where light is reflected to obtain the different masseurs (adapted from Raman Spectroscopy from an Engineering Point of View) (36)

3.2.Synthesis of MWCNT/PVP with COF in Germany

The development of the compound was carried out in 2019 at the Freie Universität Berlin in Germany by the physicist Bermeo R., the process was developed in two parts: a) formation of fibers with PVP/MWCNTs and b) synthesis of COF NP with different sizes.

3.1.1 COF NP synthesis

For the development of the COF NPs, the materials (Co(acac)₃ (1 mmol), Fe(acac)₃ (2 mmol), 1,2-hexadecanediol (10 mmol), oleic acid (6 mmol), oleylamine (6 mmol), and phenyl ether (20 ml)) in a container to later have the gasification treatment. In this case, the benzyl was substituted, as mentioned in the bibliography, by phenyl, with a very similar molecular structure. (Fig. 37)

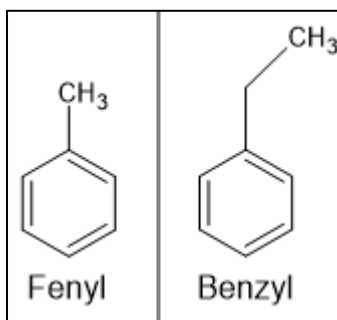


Figure 37. Similitudes between phenyl and benzyl. (adapted from Organic Chemistry)

To generate the NPs, 4 mL of hexane was added and the mixture was heated to 200 °C; then the two processes were heated with the reflux technique at 234 °C for 30 min. Finally, it was cooled to room temperature, so that the NPs stabilized, and 40 ml of ethane was added to precipitate the material, with which the COF NPs were obtained by centrifugation. The size of the NPs depends on the time and temperature of the treatment applied.

3.1.1. PVP/MWCNTs synthesis

For the synthesis of the fibers, electrospinning was used, where voltage was applied and continuous fibers were generated with the MWCNTs. MWCNTs of different layers, ranging from 5 to 25 layers of CNTs, were used in this experiment. Initially, samples were made with three ingredients: MWCNTs/NPs/PVP, PVP/DMF at 15% and PVP/ethanol at 15%, with the aim of functionalizing the PVP and MWCNTs. Furthermore, the amount in grams of each compound ranged from 2g to 4g, except for MWCNT/NPs/PVP which ranged from 0.5g to 1g.

The molecular weight of PVP ranged from 30 to 1,300 kD, with a concentration of only 15%. The voltage applied to each sample ranged from 15.41 kV to 12.91 kV. The distance obtained in the fibers was 16.3 cm. When using the electrospin machine, the production rate of milliliters per hour (ml/h) was 0.5 ml, for this reason it took approximately 2.5 to 3 h to produce a fiber with 1.5 ml. Finally, the solvents in 1 ml MWCNTs contain 0.1 DMF and 1 ml PVP contains 0.1 ml DMF. ((Fig. 38)



Figure 38. Electrospinning machines with principal components: needle, (b) pump, (c) camera and (d) square collector covered with aluminum.

3.1.2. PVP/MWCNTS characterization in Germany

The characterization was performed with Raman Spectroscopy, with the most important peaks of the already mentioned bands (G, D,2D). The values obtained were 1321, 1572 and 2713 (cm-1). For this characterization, a laser with a length of 785 nm is used. In addition, it had frequency ranges of 1250-1750 cm-1 and dim values in the other two peaks. Finally, to have an optical analysis of the fibers, TEM was used to observe the morphology of the MWCNTs/PVP, and determine the correct formation.

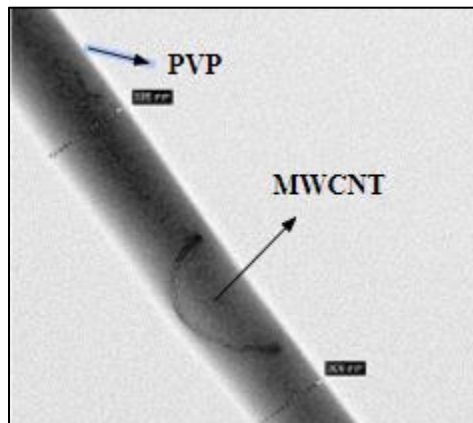


Figure 39. PVP with internal MWCNT, result from experiment analyzed in TEM

Chapter 4

4. Results & Discussion

4.1 Raman spectra and microscope images

In the study of the samples, microscope images and Raman spectroscopy were used to characterize the compounds obtained. Green laser with a wavelength of 532 nm and magnification was used for microscope images at 100x magnification. For this, the Raman LabRam HR Evolution spectrophotometer, from the Physics laboratory at Yachay Tech University, provided the data for the interpretation of the characteristics of the compounds PVP/Ethanol, PVP/MWCNTs/Ethanol, PVP/MWCNTs/CoFe₂O₄/Ethanol (CoFe₂O₄ 5-25nm). In addition, the LabSpec6 program graphs the Raman and microscope images.

An important point of the characterization is the solvent in which each studied compound was diluted, which in this case was DMF and ethanol, which will show certain repeated peaks that will have little relevance to study PVP, MWCNTs and CoFe₂O₄ with greater interest.

4.1.1. PVP Raman spectra and microscope images

The Raman and microscope images plot of the PVP showed us the expected image according to the bibliography obtained and based on its molecular structures. The most important and relevant Raman shifts for the PVP had values from 560 to 3700. (Fig. 40)

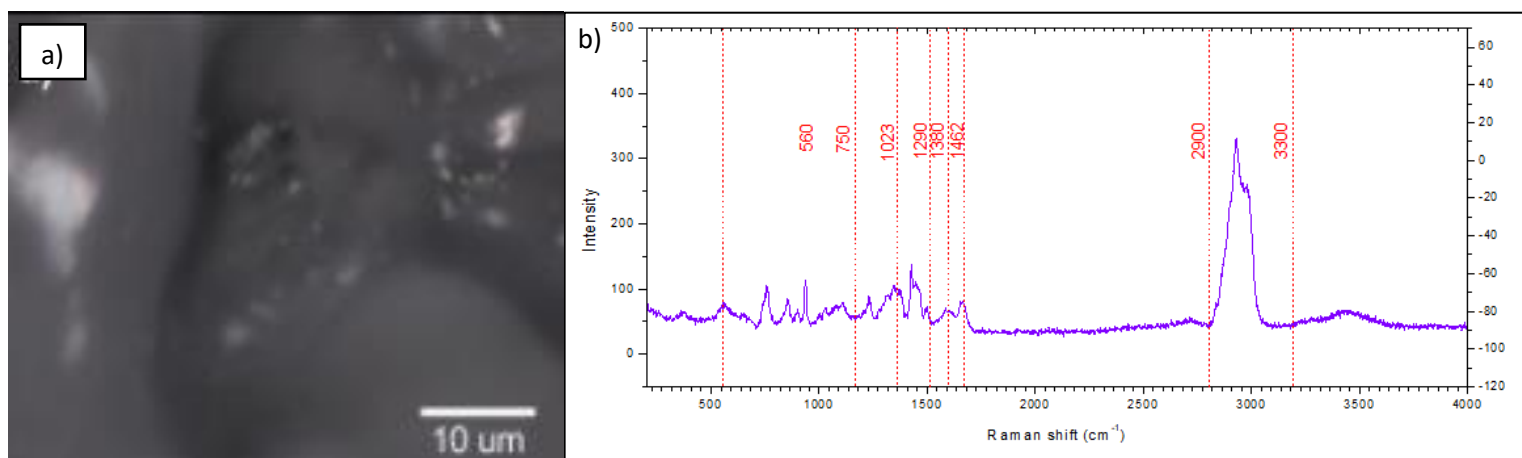


Fig 40. PVP Raman spectra a) shows microscope images of the PVP, the green point is the area where the Raman spectroscopy data were obtained; b) Raman spectroscopy of the PVP

For each Raman shift value, it is understood that they represent different PVP bonds, but they will also have other peaks where values for ethanol appear. In the obtained value of 560 cm⁻¹ it shows the double bonds of C five with the double bond of O; in addition, from the N bond in the pyrrole ring. Values from 750 to 1023 show the C bonds of the pyrrole ring for Cs 1-4, and the twist vibration for the CH₂ molecule. For the wag vibrations of CH₂ and stretch of the bond between C and N, a value of 1290 was obtained. The vibration values of bend CH and scissor Ch₂ are 1380 and 1462, respectively. Values from 2860 to 2900 show asymmetric vibrations in stretch, chain and ring of CH₂ Finally, the value of 3300 shows the bond of C with O.

4.1.2. MWCNTs/PVP Raman spectra and microscope images

The characterization of the MWCNTs/PVP showed the expected peak values according to the studies carried out by RC Avances journal. In these graphs you will also see small fibers in the microscope images image showing how a clear precision of PVP is generated, but without having a clear observation of MWCNT. (Fig. 41)

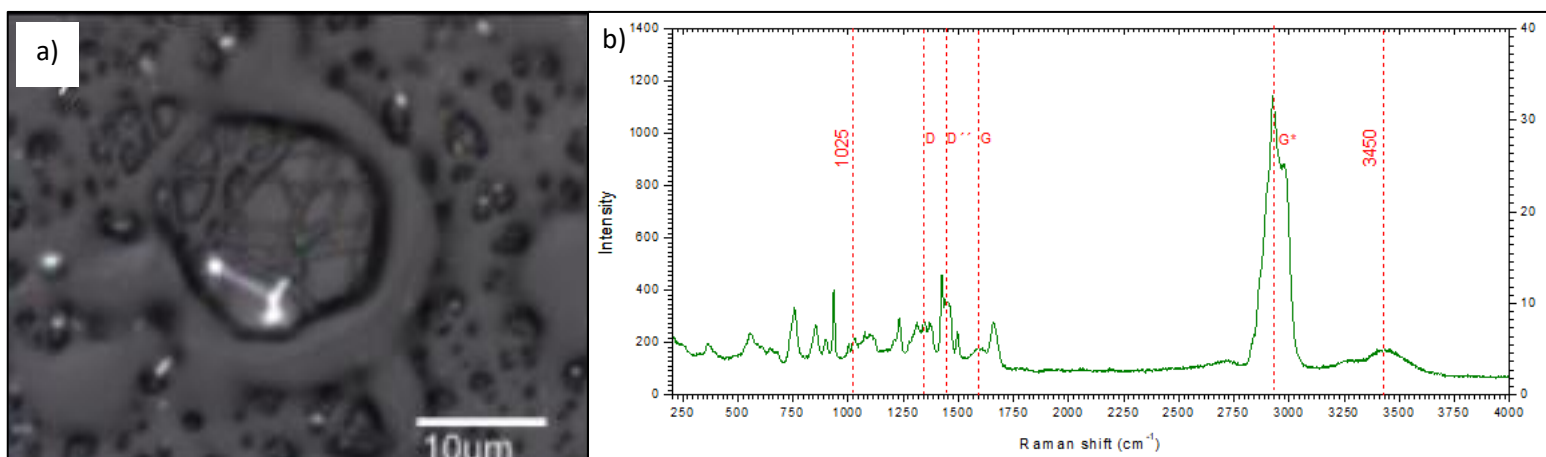


Figure 41. MWCNTs/PVP Raman spectra a) shows the microscope image of the MWCNTs/PVP, the green point is the area where the Raman spectroscopy data were obtained; b) Raman spectroscopy of the MWCNTs/PVP

For the section of the Raman graphs, the values shown in fig j and fig k are the same for the PVP peaks. On the other hand, the MWCNTs show some additional important values highlighted that the new peaks detected at 2950 cm⁻¹ and 3450 cm⁻¹ correspond to the O-H of acid and alcohol. The peak existed at 1030 cm⁻¹ and could be attributed to the primary alcohol OH (1025-1060 cm⁻¹). These peaks confirmed the binding of acid and alcohol functional groups on the MWCNT surface.

There are three sharp peaks observed in each NC at 1600, 2850 and 3400 cm⁻¹. These peaks belong to a tertiary amide, alcohol and OH of acids, respectively. To confirm the existence of hydrogen bonding, one can observe that peaks became broadened or sharpened and moved to lower absorption frequency 54. Compared to the Raman spectra of MWMCT and PVP, the peak at 3400

cm-1 was changed and broadened. Also, the presence of a sharp peak at 1640 cm-1 confirmed the presence of hydrogen bonding in all NCs.

4.1.2. MWCNTs/PVP/CoFe₂O₄ Raman spectra and microscope images

Once the individual characterization of PVP and MWCNTs/PVP was obtained, the study of the compound with COF NPs, specifically the CoFe₂O₄ molecule, was carried out. To analyze the usefulness of the NPs in detail, the size of each one was varied, totaling 4 sizes: 5, 10, 15, and 25 nm. (Fig. 42)

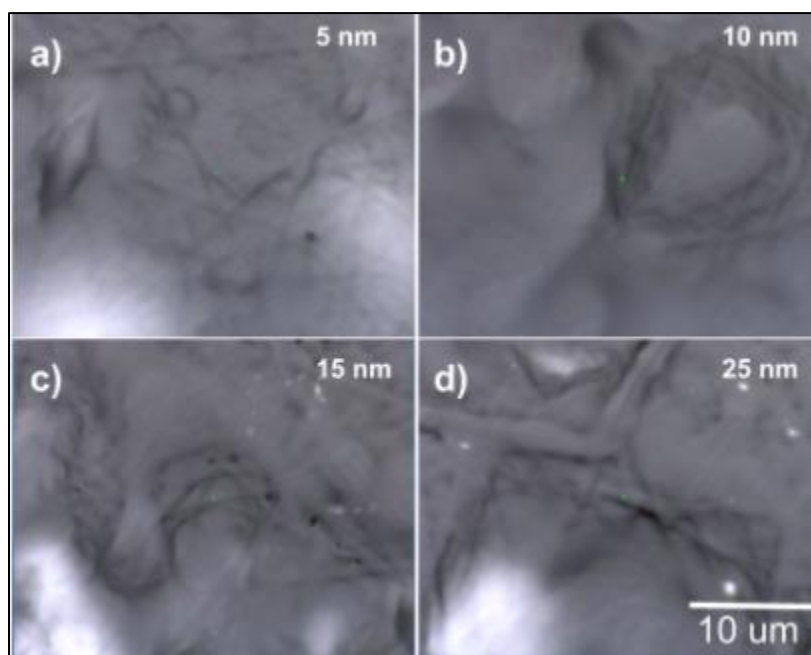


Figure 42. MWCNTs/PVP microscope image with COF NPs a) fibers with NPs of 5 nm; b) fibers with NPs of 10 nm; c) fibers with NPs of 15 nm and d) fibers with NPs of 25 nm

COF NPs improve dispersion gradually, comparing the images obtained in fig 42. First, the dispersion made by the NP with 5 nm is observed, where the fibers are observed with some difficulty, and there are not so many PVP agglomerations in the samples. (fig. 42a) The fibers that were added 10 nm showed a more proportional dispersion, in this way an agglomerate with several

fibers was found, despite this it continues to condense in certain areas that prevent a clear visualization of the fibers. (fig. 42b)

With the NPs of 15 nm the fibers were more visible and easier to find; the agglomerations showed more defined fiber reliefs. In addition, the agglomeration of the NPs with a clear distinction of white points were observed, showing that the dispersion was not as effective for the NPs. (fig. 42c) Finally, the NPs with 25 nm showed a greater dispersion for each fiber, but they had fibers that were too large in size, thus showing that the agglomeration of different fibers was growing and avoiding a more uniform formation. In this case, the much larger agglomerations of the NPs are also visualized, so there is not a great dispersion of these NPs. (fig. 42d)

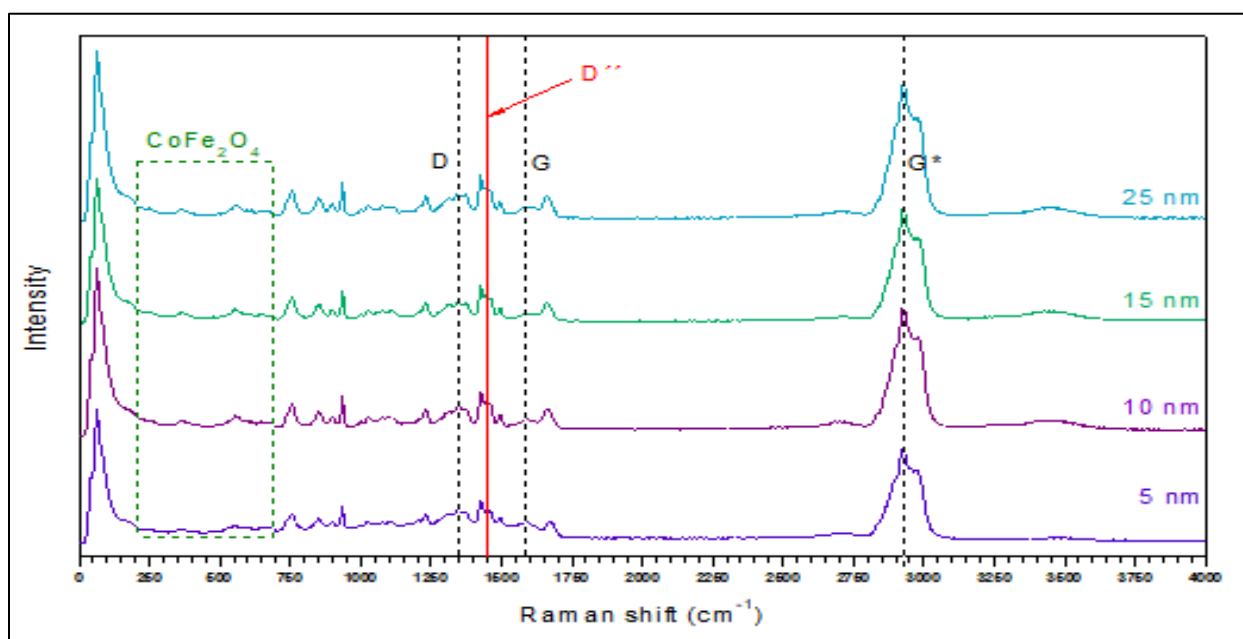


Figure 43. Raman spectra of MWCNT/PVP with COF in each different size (5,10,15 and25 nm)

Sample of the figure 43 m is the Raman spectrum of the four different samples with the variation of the size of the COF compound. The green box shows the different peaks obtained from the COF ranging from 210-695 cm^{-1} . In turn, the values of 1360 and 1586 are marked, representing the bands D (sp^3 -coordinated) and G (sp^2 -coordinated) respectively. And the value of 2650 is categorized as G* of the compound.

When comparing the four Raman spectroscopy graphs, there is no clear difference between their values, so this study would only help us determine the existing bonds, without seeing an alteration in the compound.

On the other hand, there are two clear differences in the bonds found in the graphs mentioned above, which are at 1600 and 2850 cm^{-1} . These values show a small increase in both peaks but are perceptible to understand and determine the links formed between MWCNTs and PVP. In addition, the peak between 2900 and 3100 showed an increase in the width of the graph, which is determined in this area by the OH bonds of acids, which may have increased due to the dispersion provided by the NPs, thus improving the study and determination of the compound by characterizing it in Raman.

The most relevant value of the graph is D'' zone, which was approximately 1450 cm^{-1} . This value shows the vibration of the bond between the hydrogen of the quarter carbon of the VP, with the carbon of the surface layer of the MWCNTs. In this way, check the hydrogen bonding of the PVP with the MWCNTs in the intensity increase in this D'' zone.

Chapter 5

5. Conclusions

The data collected from the bibliography and from the experiments characterized in Germany, it was possible to have a good point of view for the expected results in the characterization of the project. In addition, the number of samples helped to understand their physical characteristics and determine the status of the compounds studied. In this way, the objective was fulfilled and with results very similar to those carried out at the University of Berlin.

For the microscope image, it was a bit complex to determine the appearance of the structure, for two main reasons. The first was the limitation of observation, using a microscope magnification of a maximum range of 100x. For this reason, the majority of images showed conglomerates that did not allow the mesh of the fibers to be clearly appreciated. The second limitation comes from the state of the samples and the number of solvents and NP that were added in the synthesis process. From this point of view, the observation obtained is not unexpected, since both the DMF, ethane and COF NPs could greatly change the generation of the fibers and the NPs especially showed aggregations in which they had a measurement of 25 nm, limiting the individual study of each MWCNT/PVP fiber.

On the other hand, the Raman spectroscopy study was even more challenging. The general graphs of the intensity in relation to Raman shift, showed identical similarities in their characterization, which when viewing the graphs were practically the same. To resolve this problem, each wavelength value where a change would be expected was studied in detail, based on the literature. The most significant change was in two specific values, which improved the differentiation of plots, 1450 cm^{-1} . This peak was slightly more pronounced in the presence of MWCNTs.

On the other hand, the scope and application of this compound leaves a large opening for future research, since it was found that the field of research ranges from medicines to nanogels, as well as applicable in other production industries. Each individual compound (PVP, MWCNT and COF NP) showed to have applications in the area of medicine, but the combination of these three compounds showed much higher resistance and conductivity; Although the studies are not excessive, the applications of the PVP/MWCNT/COF compound determined that its better dispersion and addition can substitute some of the products that are currently used but individual.

Bibliography

1. Theodore M, Hosur M, Thomas J, Jeelani S. Influence of functionalization on properties of MWCNT-epoxy nanocomposites. *Materials Science and Engineering A*. 2011 Jan 25;528(3):1192–200.
2. Eitan A, Fisher FT, Andrews R, Brinson LC, Schadler LS. Reinforcement mechanisms in MWCNT-filled polycarbonate. *Compos Sci Technol*. 2006;66(9):1162–73.
3. Teodorescu M, Bercea M, Morariu S. Biomaterials of PVA and PVP in medical and pharmaceutical applications: Perspectives and challenges. Vol. 37, *Biotechnology Advances*. Elsevier Inc.; 2019. p. 109–31.
4. Xu G, Zhang Q, Zhou W, Huang J, Wei F. The feasibility of producing MWCNT paper and strong MWCNT film from VACNT array. In: *Applied Physics A: Materials Science and Processing*. 2008. p. 531–9.
5. Miranda A, Barekar N, McKay BJ. MWCNTs and their use in Al-MMCs for ultra-high thermal conductivity applications: A review. Vol. 774, *Journal of Alloys and Compounds*. Elsevier Ltd; 2019. p. 820–40.
6. Yu N, Zhang ZH, He SY. Fracture toughness and fatigue life of MWCNT/epoxy composites. *Materials Science and Engineering A*. 2008 Oct 25;494(1–2):380–4.
7. Avilés F, Cauich-Rodríguez J V., Moo-Tah L, May-Pat A, Vargas-Coronado R. Evaluation of mild acid oxidation treatments for MWCNT functionalization. *Carbon N Y*. 2009 Nov;47(13):2970–5.
8. Zulfiqar, Afzal S, Khan R, Zeb T, Rahman M ur, Burhanullah, et al. Structural, optical, dielectric and magnetic properties of PVP coated magnetite (Fe₃O₄) nanoparticles. *Journal of Materials Science: Materials in Electronics*. 2018 Dec 1;29(23):20040–50.
9. Zhang Z, Zhao B, Hu L. PVP Protective Mechanism of Ultrafine Silver Powder Synthesized by Chemical Reduction Processes. Vol. 121, *JOURNAL OF SOLID STATE CHEMISTRY*. 1996.

10. Roy N, Saha N. PVP-based hydrogels: Synthesis, properties and applications [Internet]. Available from: <https://www.researchgate.net/publication/286215035>
11. Nippon Shokubai. PVP: Polyvinylpyrrolidone [Internet]. 1999. Available from: <https://www.shokubai.co.jp/en/products/detail/pvp.html>
12. Covaliu CI, Jitaru I, Paraschiv G, Vasile E, Biriş SŞ, Diamandescu L, et al. Core-shell hybrid nanomaterials based on CoFe₂O₄ particles coated with PVP or PEG biopolymers for applications in biomedicine. *Powder Technol.* 2013 Mar;237:415–26.
13. Kurakula M, Rao GSNK. Pharmaceutical assessment of polyvinylpyrrolidone (PVP): As excipient from conventional to controlled delivery systems with a spotlight on COVID-19 inhibition. Vol. 60, *Journal of Drug Delivery Science and Technology*. Editions de Sante; 2020.
14. Dai M, Jin S, Nugen SR. Water-soluble electrospun nanofibers as a method for on-chip reagent storage. *Biosensors (Basel)*. 2012;2(4):388–95.
15. Dong F, Wan J, Feng Y, Wang Z, Ni J. Experimental Study on Thermophysical Properties of Propylene Glycol-Based Graphene Nanofluids. *Int J Thermophys.* 2021 Apr 1;42(4).
16. Teodorescu M, Bercea M. Poly(vinylpyrrolidone) – A Versatile Polymer for Biomedical and Beyond Medical Applications. *Polymer - Plastics Technology and Engineering*. 2015 Jun 23;54(9):923–43.
17. Chemical Abstracts Service. Poly(vinylpyrrolidone). Chemical Abstracts Service. 2022 Jan 29;
18. Cerveny S, Colmenero J, Alegría A. Dielectric investigation of the low-temperature water dynamics in the poly(vinyl methyl ether)/H₂O system. *Macromolecules*. 2005 Aug 9;38(16):7056–63.
19. Qiao Y, Yin X, Zhu T, Li H, Tang C. Dielectric polymers with novel chemistry, compositions and architectures. Vol. 80, *Progress in Polymer Science*. Elsevier Ltd; 2018. p. 153–62.

20. Du YK, Yang P, Mou ZG, Hua NP, Jiang L. Thermal decomposition behaviors of PVP coated on platinum nanoparticles. *J Appl Polym Sci*. 2006 Jan 5;99(1):23–6.
21. Shinyashiki N, Spanoudaki A, Yamamoto W, Nambu E, Yoneda K, Kyritsis A, et al. Segmental relaxation of hydrophilic poly(vinylpyrrolidone) in chloroform studied by broadband dielectric spectroscopy. *Macromolecules*. 2011 Apr 12;44(7):2140–8.
22. Elazab HA, Ayad MN, Hammam MM, Radwan MA, Sadek MA, Radwan MA, et al. Synthesis and Characterization of PVP Based Catalysts for Synthesis and Characterization of PVP Based Catalysts for Selected Application in Catalysis Selected Application in Catalysis Synthesis and characterization of PVP based catalysts for selected application in catalysis. Available from: https://buescholar.bue.edu.eg/chem_eng/96
23. Fischer F, Bauer S. Ein Tausendsassa in der Chemie: Polyvinylpyrrolidon. *Chemie in Unserer Zeit*. 2009 Dec;43(6):376–83.
24. Bhat R. SYNTHESIS AND STRUCTURE-PROPERTY CORRELATIONS OF γ -SUBSTITUTED PYRROLIDONE-BASED POLYMERS. 2017.
25. Wang H, Qiao X, Chen J, Wang X, Ding S. Mechanisms of PVP in the preparation of silver nanoparticles. Vol. 94, *Materials Chemistry and Physics*. 2005. p. 449–53.
26. prado_abellan_anselmo_del.
27. Nowak B (inżynieria chemiczna), Werner Łukasz, Wierzba P (inżynieria chemiczna), Politechnika Warszawska. Koło Naukowe Inżynierii Chemicznej i Procesowej., Fundacja Młodej Nauki. EYEC monograph : 6th European Young Engineers Conference, April 24-26th 2017, Warsaw. Faculty of Chemical and Process Engineering, Warsaw University of Technology; 2017.
28. Zhang AQ, Cai LJ, Sui L, Qian DJ, Chen M. Reducing properties of polymers in the synthesis of noble metal nanoparticles. *Polymer Reviews*. 2013 May 1;53(2):240–76.
29. Xiong Y, Washio I, Chen J, Cai H, Li ZY, Xia Y. Poly (vinyl pyrrolidone): A dual functional reductant and stabilizer for the facile synthesis of noble metal nanoplates in aqueous solutions. *Langmuir*. 2006 Sep 26;22(20):8563–70.

30. Hoppe CE, Lazzari M, Pardiñas-Blanco I, López-Quintela MA. One-step synthesis of gold and silver hydrosols using poly(N-vinyl-2-pyrrolidone) as a reducing agent. *Langmuir*. 2006 Aug 1;22(16):7027–34.
31. Amin PD, Bhanushali V, Joshi S. Role of Polyvinylpyrrolidone in Membrane Technologies. *Int J Chemtech Res*. 2018;11(9):247–59.
32. Chemical book. Polyvinylpyrrolidone. 2016. Polyvinylpyrrolidone.
33. Hiremath P, Nuguru K, Agrahari V. Material attributes and their impact on wet granulation process performance. In: *Handbook of Pharmaceutical Wet Granulation: Theory and Practice in a Quality by Design Paradigm*. Elsevier; 2018. p. 263–315.
34. LD5655.V855_1996.L536.
35. PRODUCT DATA Ashland Specialty Ingredients PVP K-15 polymer PVP K-15. 2013.
36. Irfan M, Irfan M, Shah SM, Baig N, Saleh TA, Ahmed M, et al. Hemodialysis performance and anticoagulant activities of PVP-k25 and carboxylic-multiwall nanotube composite blended Polyethersulfone membrane. *Materials Science and Engineering C*. 2019 Oct 1;103.
37. Jouyandeh M, Ali JA, Akbari V, Aghazadeh M, Paran SMR, Naderi G, et al. Curing epoxy with polyvinylpyrrolidone (PVP) surface-functionalized $Mn_xFe_{3-x}O_4$ magnetic nanoparticles. *Prog Org Coat*. 2019 Nov 1;136.
38. Yu DG, Branford-White C, White K, Li XL, Zhu LM. Dissolution improvement of electrospun nanofiber-based solid dispersions for acetaminophen. *AAPS PharmSciTech*. 2010 Jun;11(2):809–17.
39. Yu Z, Shi Q, Dong L, Wang H, Huang Q, Fukuda T. Contact Annealing for Self-Soldering: In Situ Investigation into Interfaces between PVP-Coated Silver Nanoelectrodes and Carbon Nanotubes. *ACS Appl Mater Interfaces*. 2019 Oct 2;11(39):36035–43.
40. Kurakula M, Rao GSNK. Pharmaceutical assessment of polyvinylpyrrolidone (PVP): As excipient from conventional to controlled delivery systems with a spotlight on COVID-19

- inhibition. Vol. 60, Journal of Drug Delivery Science and Technology. Editions de Sante; 2020.
41. Kondiah PJ, Choonara YE, Kondiah PPD, Marimuthu T, Kumar P, Du Toit LC, et al. A review of injectable polymeric hydrogel systems for application in bone tissue engineering. Vol. 21, Molecules. MDPI AG; 2016.
 42. Thomas S, Shanks R (Robert A), Joy J. Micro- and nanostructured polymer systems : from synthesis to applications.
 43. Kondiah PJ, Choonara YE, Kondiah PPD, Marimuthu T, Kumar P, Du Toit LC, et al. A review of injectable polymeric hydrogel systems for application in bone tissue engineering. Vol. 21, Molecules. MDPI AG; 2016.
 44. Ng KW, Torzilli PA, Warren RF, Maher SA. Characterization of a macroporous polyvinyl alcohol scaffold for the repair of focal articular cartilage defects. J Tissue Eng Regen Med. 2014;8(2):164–8.
 45. Belin T, Epron F. Characterization methods of carbon nanotubes: A review. Vol. 119, Materials Science and Engineering B: Solid-State Materials for Advanced Technology. 2005. p. 105–18.
 46. Zaytseva O, Neumann G. Carbon nanomaterials: Production, impact on plant development, agricultural and environmental applications. Vol. 3, Chemical and Biological Technologies in Agriculture. Springer International Publishing; 2016.
 47. Chaudhary KT, Rizvi ZH, Bhatti KA, Ali J, Yupapin PP. Multiwalled carbon nanotube synthesis using arc discharge with hydrocarbon as feedstock. J Nanomater. 2013;2013.
 48. Saifuddin N, Raziah AZ, Junizah AR. Carbon nanotubes: A review on structure and their interaction with proteins. J Chem. 2013;
 49. Jonathan Clayden NG and SW. Organic Chemistry. 2012.
 50. Miao Z, Wang D. An Electrically and Thermally Erasable Liquid Crystal Film Containing NIR Absorbent Carbon Nanotube. Molecules. 2022 Jan 1;27(2).

51. Escobar M, Moreno MS, Candal RJ, Marchi MC, Caso A, Polosecki PI, et al. Synthesis of carbon nanotubes by CVD: Effect of acetylene pressure on nanotubes characteristics. *Appl Surf Sci.* 2007 Oct 31;254(1 SPEC. ISS.):251–6.
52. Solhy A, Machado BF, Beausoleil J, Kihn Y, Gonçalves F, Pereira MFR, et al. MWCNT activation and its influence on the catalytic performance of Pt/MWCNT catalysts for selective hydrogenation. *Carbon N Y.* 2008 Aug;46(9):1194–207.
53. Thostenson ET, Ren Z, Chou TW. Advances in the science and technology of carbon nanotubes and their composites: a review [Internet]. Available from: www.elsevier.com/locate/compscitech
54. Aliev AE, Guthy C, Zhang M, Fang S, Zakhidov AA, Fischer JE, et al. Thermal transport in MWCNT sheets and yarns. *Carbon N Y.* 2007 Dec;45(15):2880–8.
55. Lim SH, Li Z, Poh CK, Lai L, Lin J. Highly active non-precious metal catalyst based on poly(vinylpyrrolidone)- wrapped carbon nanotubes complexed with iron-cobalt metal ions for oxygen reduction reaction. *J Power Sources.* 2012 Sep 15;214:15–20.
56. Maziukiewicz D, Maciejewska BM, Litowczenko J, Kościński M, Warowicka A, Wychowaniec JK, et al. Designing biocompatible spin-coated multiwall carbon nanotubes-polymer composite coatings. *Surf Coat Technol.* 2020 Mar 15;385.
57. Boumia L, Zidour M, Benzair A, Tounsi A. A Timoshenko beam model for vibration analysis of chiral single-walled carbon nanotubes. *Physica E Low Dimens Syst Nanostruct.* 2014 May;59:186–91.
58. Ra EJ, An KH, Kim KK, Jeong SY, Lee YH. Anisotropic electrical conductivity of MWCNT/PAN nanofiber paper. *Chem Phys Lett.* 2005 Sep 15;413(1–3):188–93.
59. Irfan M, Idris A, Yusof NM, Khairuddin NFM, Akhmal H. Surface modification and performance enhancement of nano-hybrid f-MWCNT/PVP90/PES hemodialysis membranes. *J Memb Sci.* 2014 Oct 1;467:73–84.
60. Sengupta A, Gupta NK. MWCNTs based sorbents for nuclear waste management: A review. Vol. 5, *Journal of Environmental Chemical Engineering.* Elsevier Ltd; 2017. p. 5099–114.

61. Saeb MR, Bakhshandeh E, Khonakdar HA, Mäder E, Scheffler C, Heinrich G. Cure kinetics of epoxy nanocomposites affected by MWCNTs functionalization: A review. *The Scientific World Journal*. 2013;2013.
62. Serrano MC, Nardecchia S, García-Rama C, Ferrer ML, Collazos-Castro JE, Del Monte F, et al. Chondroitin sulphate-based 3D scaffolds containing MWCNTs for nervous tissue repair. *Biomaterials*. 2014 Feb;35(5):1543–51.
63. Kim TH, Kwon CH, Lee C, An J, Phuong TTT, Park SH, et al. Bio-inspired hybrid carbon nanotube muscles. *Sci Rep*. 2016 May 25;6.
64. Ntim SA, Sae-Khow O, Witzmann FA, Mitra S. Effects of polymer wrapping and covalent functionalization on the stability of MWCNT in aqueous dispersions. *J Colloid Interface Sci*. 2011 Mar 15;355(2):383–8.
65. Lee SH, Kim MW, Kim SH, Youn JR. Rheological and electrical properties of polypropylene/MWCNT composites prepared with MWCNT masterbatch chips. *Eur Polym J*. 2008 Jun;44(6):1620–30.
66. Gangu KK, Maddila S, Mukkamala SB, Jonnalagadda SB. Characteristics of MOF, MWCNT and graphene containing materials for hydrogen storage: A review. *Journal of Energy Chemistry*. Elsevier B.V.; 2019. p. 132–44.
67. Lai X, Yost BLB, Clack JW, Fears SL, Mitra S, Ntim SA, et al. Protein expression profiles of intestinal epithelial co-cultures: effect of functionalised carbon nanotube exposure. *Int J Biomed Nanosci Nanotechnol*. 2013;3(1/2):127.
68. Bernal-Martinez J, Godínez-Fernández R, Aguilar-Elguezabal A. Suitability of the Composite Made of Multi Wall Carbon Nanotubes-Polyvinylpyrrolidone for Culturing Invertebrate <i>Helix aspersa</i> Neurons. *Journal of Materials Science and Chemical Engineering*. 2017;05(02):41–50.
69. Cote LJ, Teja AS, Wilkinson AP, Zhang ZJ. Continuous hydrothermal synthesis of CoFe₂O₄ nanoparticles. In: *Fluid Phase Equilibria*. Elsevier; 2003. p. 307–17.

70. Shi Y, Ding J, Yin H. CoFe O nanoparticles prepared by the mechanochemical method 2 4 [Internet]. Vol. 308, Journal of Alloys and Compounds. 2000. Available from: www.elsevier.com/locate/jallcom
71. Hashim A, Habeeb MA. Synthesis and Characterization of Polymer Blend-CoFe 2 O 4 Nanoparticles as a Humidity Sensors for Different Temperatures. Transactions on Electrical and Electronic Materials. 2019 Apr 5;20(2):107–12.
72. Qu Y, Yang H, Yang N, Fan Y, Zhu H, Zou G. The effect of reaction temperature on the particle size, structure and magnetic properties of coprecipitated CoFe₂O₄ nanoparticles. Mater Lett. 2006 Dec;60(29–30):3548–52.
73. Liu C, Rondinone AJ, Zhang ZJ. Synthesis of magnetic spinel ferrite CoFe 2 O 4 nanoparticles from ferric salt and characterization of the size-dependent superparamagnetic properties*. Vol. 72, Pure Appl. Chem. 2000.
74. Jalalian M, Mirkazemi SM, Alamolhoda S. Phase constituents and magnetic properties of the CoFe₂O₄ nanoparticles prepared by polyvinylpyrrolidone (PVP)-assisted hydrothermal route. Appl Phys A Mater Sci Process. 2016 Sep 1;122(9).
75. Limaye M V., Singh SB, Date SK, Kothari D, Reddy VR, Gupta A, et al. High coercivity of oleic acid capped CoFe₂O₄ nanoparticles at room temperature. Journal of Physical Chemistry B. 2009 Jul 9;113(27):9070–6.
76. Novis Y, De Meulemeester R, Chtai' M, Pireaux JJ, Caudano R. XPS and SEM Study of UV Laser Surface Modification of Polymers. Vol. 21, British Polymer Journal. 1989.
77. Grafov A, Vuorinen S, Repo T, Kemell M, Nieger M, Leskelä M. New Sn(IV) and Ti(IV) bis(trimethylsilyl)amides in d,l-lactide polymerization, SEM characterization of polymers. Eur Polym J. 2008 Nov;44(11):3797–805.
78. Agarwal UP, Ralph SA. FT-Raman Spectroscopy of Wood: Identifying Contributions of Lignin and Carbohydrate Polymers in the Spectrum of Black Spruce (*Picea mariana*). Vol. 51, APPLIED SPECTROSCOPY. 1997.
79. Movasaghi Z, Rehman S, Rehman IU. Raman spectroscopy of biological tissues. Vol. 42, Applied Spectroscopy Reviews. 2007. p. 493–541.

80. Tomikawa K, Kanno H, Kimoto H. A Raman study of aqueous DMF and DMA solutions at low temperatures. *Can J Chem*. 2004 Oct;82(10):1468–73.
81. van Duyne RP, Hulteen JC, Treichel DA. Atomic force microscopy and surface-enhanced Raman spectroscopy. I. Ag island films and Ag film over polymer nanosphere surfaces supported on glass. *Journal of Chemical Physics*. 1993;99(3):2101–15.